NASA TECH BRIEFS

NATIONAL AERONAUTICS AND SPACE ADMINISTRATION

⊕ **Technology Focus**

∿ **Computers/Electronics**

◑ **Software**

◼ **Materials**

☢ **Mechanics**

✱ **Machinery/Automation**

⊐ **Manufacturing**

⟨ **Bio-Medical**

⚛ **Physical Sciences**

Σ **Information Sciences**

📚 **Books and Reports**

INTRODUCTION

Tech Briefs are short announcements of innovations originating from research and development activities of the National Aeronautics and Space Administration. They emphasize information considered likely to be transferable across industrial, regional, or disciplinary lines and are issued to encourage commercial application.

Availability of NASA Tech Briefs and TSPs

Requests for individual Tech Briefs or for Technical Support Packages (TSPs) announced herein should be addressed to

National Technology Transfer Center

Telephone No. **(800) 678-6882** or via World Wide Web at **www2.nttc.edu/leads/**

Please reference the control numbers appearing at the end of each Tech Brief. Information on NASA's Commercial Technology Team, its documents, and services is also available at the same facility or on the World Wide Web at **www.nctn.hq.nasa.gov**.

Commercial Technology Offices and Patent Counsels are located at NASA field centers to provide technology-transfer access to industrial users. Inquiries can be made by contacting NASA field centers and program offices listed below.

NASA Field Centers and Program Offices

Ames Research Center
Lisa L. Lockyer
(650) 604-3009
lisa.l.lockyer@nasa.gov

Dryden Flight Research Center
Gregory Poteat
(661) 276-3872
greg.poteat@dfrc.nasa.gov

Goddard Space Flight Center
Nona Cheeks
(301) 286-5810
Nona.K.Cheeks.1@gsfc.nasa.gov

Jet Propulsion Laboratory
Ken Wolfenbarger
(818) 354-3821
james.k.wolfenbarger@jpl.nasa.gov

Johnson Space Center
Charlene E. Gilbert
(281) 483-3809
commercialization@jsc.nasa.gov

Kennedy Space Center
Jim Aliberti
(321) 867-6224
Jim.Aliberti-1@ksc.nasa.gov

Langley Research Center
Jesse Midgett
(757) 864-3936
jesse.c.midgett@nasa.gov

John H. Glenn Research Center at Lewis Field
Larry Viterna
(216) 433-3484
cto@grc.nasa.gov

Marshall Space Flight Center
Vernotto McMillan
(256) 544-2615
vernotto.mcmillan@msfc.nasa.gov

Stennis Space Center
Robert Bruce
(228) 688-1929
robert.c.bruce@nasa.gov

NASA Program Offices

At NASA Headquarters there are seven major program offices that develop and oversee technology projects of potential interest to industry:

Carl Ray
Small Business Innovation Research Program (SBIR) & Small Business Technology Transfer Program (STTR)
(202) 358-4652 or
cray@nasa.gov

Benjamin Neumann
InnovativeTechnology Transfer Partnerships (Code TD)
(202) 358-2320
benjamin.j.neumann@nasa.gov

John Mankins
Office of Space Flight (Code TD)
(202) 358-4659 or
john.c.mankins@nasa.gov

Terry Hertz
Office of Aero-Space Technology (Code RS)
(202) 358-4636 or
thertz@nasa.gov

Glen Mucklow
Office of Space Sciences (Code SM)
(202) 358-2235 or
gmucklow@nasa.gov

Roger Crouch
Office of Microgravity Science Applications (Code U)
(202) 358-0689 or
rcrouch@nasa.gov

Granville Paules
Office of Mission to Planet Earth (Code Y)
(202) 358-0706 or
gpaules@mtpe.hq.nasa.gov

Tech Briefs

NATIONAL AERONAUTICS AND SPACE ADMINISTRATION

Instrumentation for Sensitive Gas Measurements

Measurements are based on cavity-enhanced absorption.

Ames Research Center, Moffett Field, California

An improved instrument for optical absorption spectroscopy utilizes off-axis paths in an optical cavity in order to increase detection sensitivity while suppressing resonance effects. The instrument is well suited for use in either cavity ring-down spectroscopy (CRDS) [in which one pulses an incident light beam and measures the rate of decay of light in the cavity] or integrated cavity output spectroscopy (ICOS) [in which one uses a continuous-wave incident light beam and measures the power of light in the cavity as a function of wavelength].

Typically, in optical absorption spectroscopy, one seeks to measure absorption of a beam of light in a substance (usually a gas or liquid) in a sample cell. In CRDS or ICOS, the sample cell is placed in (or consists of) an optical cavity, so that one can utilize multiple reflections of the beam to increase the effective optical p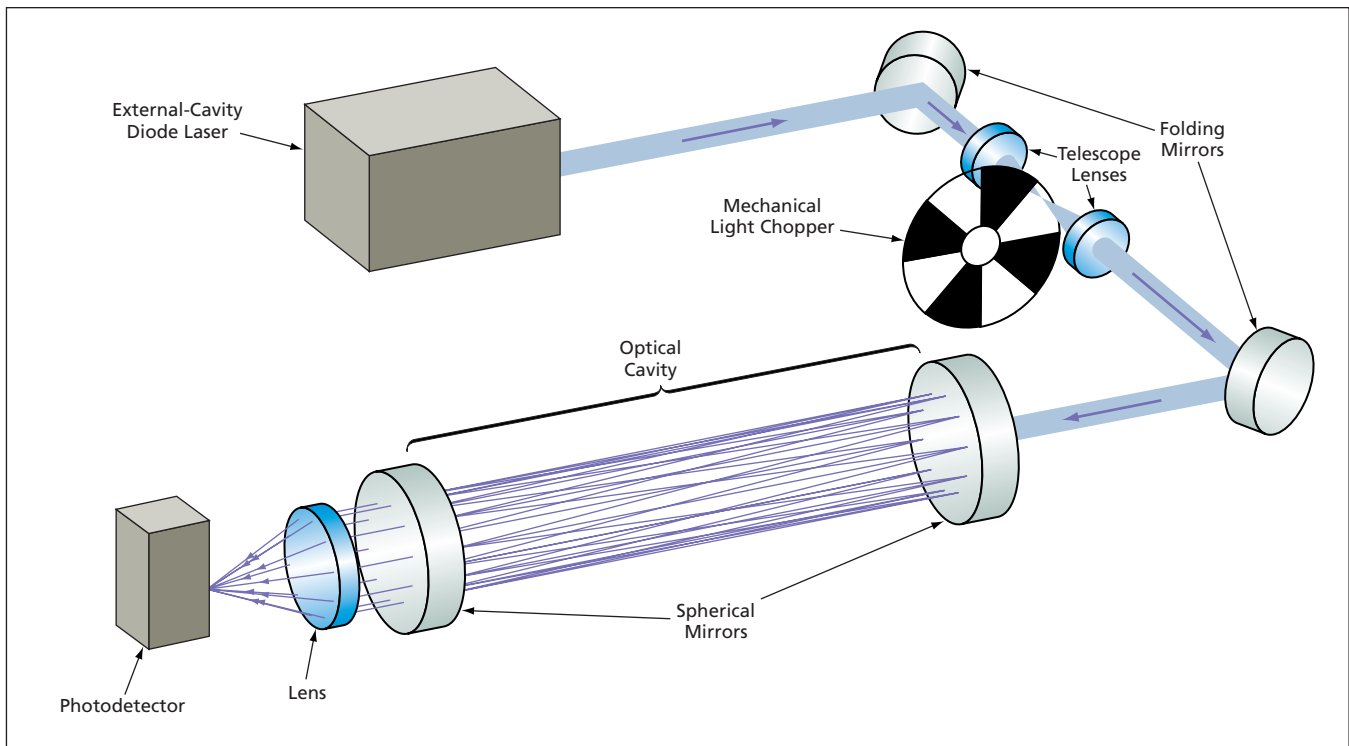ath length through the absorbing substance and thereby increase the sensitivity for measuring absorption. If an absorbing substance is not present in the optical cavity, one can utilize the multiple passes of the light beam to increase the sensitivity for measuring absorption and scattering by components of the optical cavity itself.

It is desirable to suppress the effects of resonances in the cavity in order to make the spectral response of the cavity itself as nearly constant as possible over the entire wavelength range of interest. In the present instrument, the desired flattening of the spectral response is accomplished by utilizing an off-axis beam geometry to effectively decrease the frequency interval between longitudinal electromagnetic modes of the cavity, such that the resulting transmission spectrum of the cavity is nearly continuous: in other words, the cavity becomes a broad-band optical device.

The instrument (see figure) includes an external-cavity diode laser, the output of which is directed by folding mirrors into an optical cavity. Optionally, the electromagnetic modes of the laser and the cavity can be matched by use of two telescope lenses. Also, optionally, the laser beam can be chopped for (CRDS) or not chopped (for ICOS). The optical cavity is bounded by two identical mirrors, typically having a diameter of 25 mm and a radius of curvature of 6 m (and, hence, a focal length of 3 m). Typically, the mirrors are longitudinally separated by a distance of 67 cm. Preferably, the mirrors both have reflectivities >0.99, though reflectivities as low as 0.5 could be acceptable in some applications.

The aforementioned choice of typical parameters — and in particular, the choice of a mirror focal length greater than the cavity length — was made on the basis of numerical simulations of a variety of cavity designs that yield dense mode spectra. The simulations showed that the long-focal-length condition minimizes the sensitivity of perfor-

The **Optical Path Through the Cavity** comprises multiple off-axis segments. With a suitable choice of design parameters, this arrangement yields a dense longitudinal-mode spectrum that offers several advantages.

mance to changes in the alignment and spacing of the mirrors. In addition, as a result of this choice of parameters, the light emerges from the cavity in a pattern that facilitates focusing of the light onto a possibly small photodetector.

The greatest advantage afforded by this design, relative to an on-axis design, is that one can use a narrow-band laser (bandwidth < 100 MHz), without need for complex, expensive equipment for precisely controlling the cavity length to manipulate or suppress resonances. Another advantage is reduction of optical feedback from the cavity to the laser and consequent elim-

ination of need for optical components to suppress such feedback.

Yet another advantage is removal of a major constraint on the alignment of the overall optical system: Instead of only one possible alignment geometry (the laser beam aligned with the optical axis of the cavity), one can choose any alignment for which there is a stable optical path through the cavity. As a result, alignment routine can be simplified and the instrument is less sensitive to vibration.

Currently, a product line of instruments is being developed based on the technology described above for high-

sensitivity, precision, and accurate gas measurements. Some applications that will benefit from this technology include atmospheric monitoring, chemical and biological agent detection, industrial process control, and medical diagnostics.

This work was done by Anthony O'Keefe of Los Gatos Research for **Ames Research Center**.

Inquiries concerning rights for the commercial use of this invention should be addressed to the Patent Counsel, Ames Research Center, (650) 604-5104. Refer to ARC-14690-1.

Apparatus for Testing Flat Specimens of Thermal Insulation
An improved design affords flexibility for testing under diverse conditions.

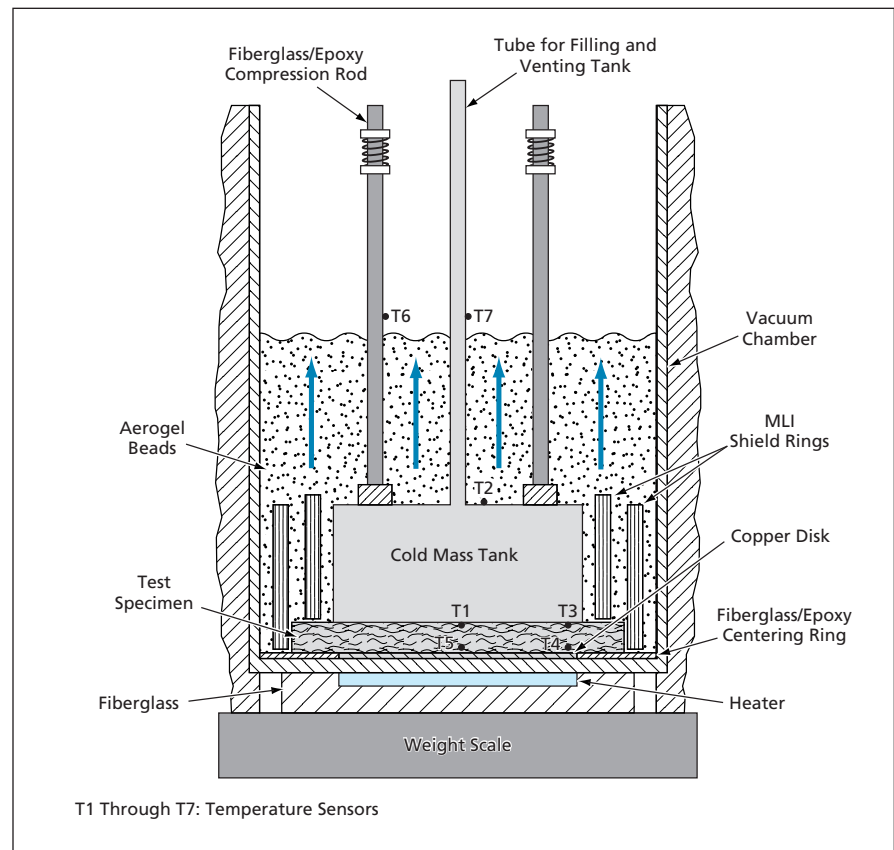*John F. Kennedy Space Center, Florida*

An apparatus has been developed to implement an improved method of testing flat-plate specimens of thermal-insulation materials for cryogenic application. The method includes testing under realistic use conditions that could include vacuum and mechanical loading at a pressure up to 70 psi (≈0.48 MPa). The apparatus can accommodate a rigid or flexible specimen having thickness up to 1.25 in. (≈3.2 cm) and diameters between 6 and 10 in. (about 15.2 and 25.4 cm, respectively). Typical test conditions include boundary temperatures between 77 K and 373 K and vacuum/interstitial gas filling at a pressure between 10^{-6} torr (≈1.3×10^{-4} Pa) and 760 torr (atmospheric pressure ≈0.1 MPa). The interstitial gas could be N_2, He, CO_2, or any other suitable gas to which the insulation is expected to be exposed in use. Relative to prior apparatuses and testing methods, this apparatus and the testing method that it implements offer advantages of relative simplicity and ease of use.

The basic principle of operation of the apparatus is that of boil-off calorimetry, using liquid nitrogen or any other suitable liquid that boils at a desired temperature below ambient temperature. Comparative rates of flow of heat through the thicknesses of the specimens (heat-leak rates) and apparent-thermal-conductivity values are obtained from tests of specimens. Absolute values of heat-leak rates and apparent thermal conductivities are computed from a combination of (1) the aforementioned comparative values and (2) calibra-

tion factors obtained by testing reference specimens of materials that have known thermal-insulation properties.

The apparatus includes a full complement of temperature sensors, a vacuum pump and chamber, a monitoring and

control system, and tools and fixtures that enable rapid and reliable installation and removal of specimens. A specimen is installed at the bottom of the vacuum chamber, and a cold-mass assembly that includes a tank is lowered into posi-

A **Specimen Is Sandwiched** between a cold mass tank containing liquid nitrogen and a heated copper plate. The apparent thermal conductivity of the specimen is determined from the liquid-nitrogen boil-off rate and the temperatures of the top and bottom specimen surfaces.

tion above and around the specimen (see figure). A spring-based compensating fixture helps to ensure adequate thermal contact with possibly irregular specimen surfaces. For a high-compression test, the springs can be replaced with spacers. A flat circular load cell at the bottom of the chamber measures the compressive load on the specimen. Once the desired compressive-load, temperature, and vacuum/gas-filling conditions are established, testing begins.

During a test, all measurements are recorded by use of a portable data-acquisition system and a computer.

The total heat-leak rate is measured and calculated as the boil-off flow rate multiplied by the latent heat of vaporization. The parasitic heat leak (to the side of the specimen and to the top and side of the cold-mass tank) is reduced to a small fraction of the total heat leak by use of a combination of multilayer-insulation (MLI) shield rings, reflective

film, a fiberglass/epoxy centering ring, and a bulk fill of aerogel beads. This combination eliminates the need for a cryogenic guard chamber used in a typical prior apparatus to reduce the parasitic heat leak.

This work was done by James E. Fesmire of **Kennedy Space Center** *and Stanislaw D. Augustynowicz of Dynacs, Inc. Further information is contained in a TSP (see page 1).*
KSC-12390

Quadrupole Ion Mass Spectrometer for Masses of 2 to 50 Da
H_2, He, O_2, and Ar can be quantitated at low concentrations in N_2.
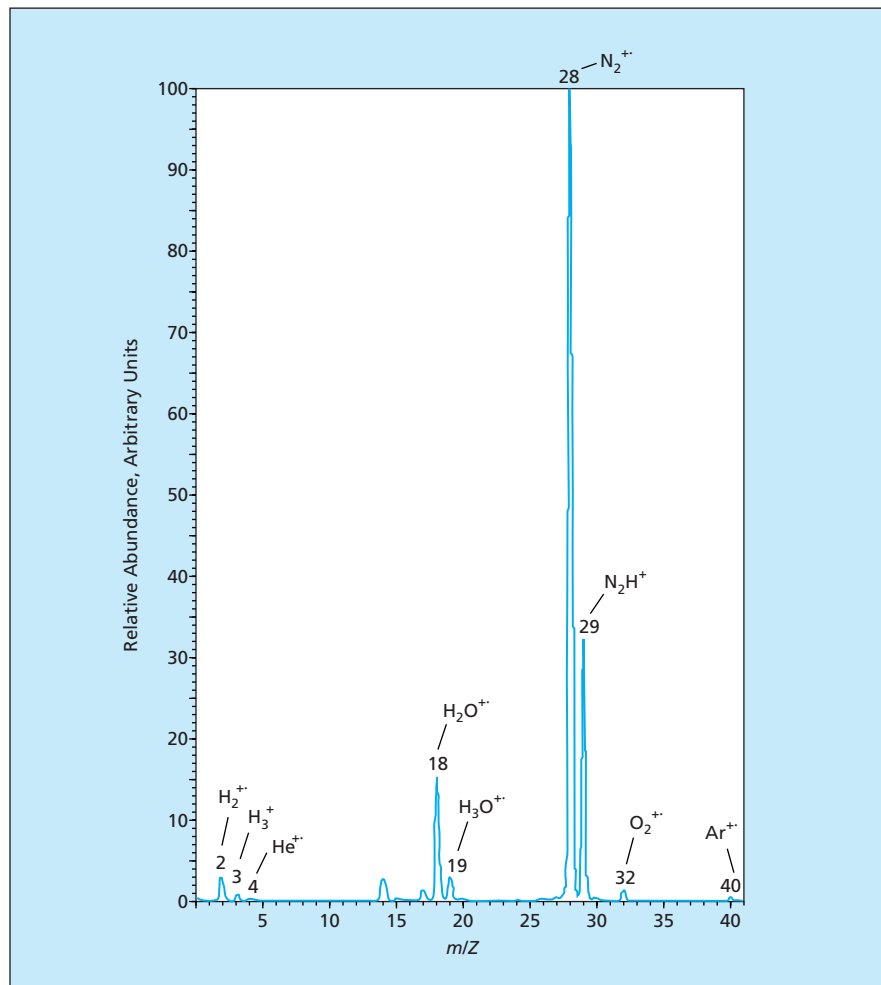
John F. Kennedy Space Center, Florida

A customized quadrupole ion-trap mass spectrometer (QITMS) has been built to satisfy a need for a compact, rugged instrument for measuring small concentrations of hydrogen, helium, oxygen, and argon in a nitrogen atmosphere. This QITMS can also be used to perform quantitative analyses of other gases within its molecular-mass range, which is 2 to 50 daltons (Da). (More precisely, it can be used to perform quantitative analysis of gases that, when ionized, are characterized by m/Z ratios between 2 and 50, where m is the mass of an ion in daltons and Z is the number of fundamental electric charges on the ion.)

The QITMS was assembled mostly from commercial components. It includes a vacuum manifold, ion trap, and filament from a commercial ion-trap mass analyzer that produces ions within the ion trap by electron impact. Low-molecular-weight ions are effectively trapped when internal electron impact is used, despite the absence of a collision (buffer) gas. This internal-electron-impact assembly is compact, rugged, and suited for use in a miniaturized instrument. The assembly was modified to (1) increase the opening of the trap to the vacuum manifold in order to increase the rates of transport of analyte gases, (2) accommodate an ion high-vacuum gauge that measures the pressure in the open ion trap, and (3) replace an original gas-chromatograph-type transfer tube with a stainless-steel tube for introducing gas samples into the trap. A high vacuum is produced in the trap by means of a turbo-drag pump backed by either a diaphragm pump or a rotary-vane pump.

The electronic control and monitoring unit of the aforementioned commercial

ion-trap mass analyzer was replaced by a more capable control and monitoring unit from another commercial ion-trap mass analyzer, with minor changes in the electron-filament portion of the replacement unit to regulate emission of electrons from the filament. With this modification, the electron-emission assembly produces a 200-μA current of electrons at a kinetic energy of 90 eV. An electron multiplier from the second-mentioned commercial ion-trap mass analyzer was in-

This **Mass Spectrum** was obtained in an initial test of the QITMS, using a mixture of H_2, He, O_2, and Ar, each at a concentration of 1.25 percent in N_2.

stalled in the vacuum manifold to match an electrometer circuit in the control and monitoring unit.

The instrument operates under control by a computer that runs custom software. Included in the software is a module for performing real-time monitoring of selected gases at a chosen update rate (e.g., once per second).

Like commercial instruments, this QITMS utilizes a mass-selective instability for mass analysis. Both commercial ion-trap analyzers from which the parts were taken to build the present unit have low-mass cutoffs of 4 Da. To extend the lower mass limit to 2 Da with the least amount of modification and fabrication, it was decided to increase the upper limit of frequency of the signal applied to coils to generate the trapping radio-frequency field. This decision was implemented through modifications of the signal-generating circuits and construction of replacement coils to provide multiple resonance frequencies from 1 to 4 MHz. Increasing the upper limit of frequency reduced the upper limit of the mass range below that of the unmodified commercial instruments, but this was acceptable because the upper mass limit of 50 Da required for this instrument remained within range.

The QITMS was initially tested at a frequency of 2.8 MHz with a sample gas mixture comprising 1.25 percent, each, of hydrogen, helium, oxygen, and argon in nitrogen. The results of this test showed readily identifiable ion signals at m/Z values of 2, 4, 32, and 40, with an upper m/Z limit only a few tenths above 40 (see figure). In a subsequent test, it was found that the desired m/Z range of 2 to 50 could be attained in operation at a frequency of 2.5 MHz. In other tests, it was found that the relative accuracy and precision in quantitating the four gases of interest were characterized by an error of no more than 10 percent of reading and a deviation of no more than 5 percent of reading, respectively. In still other tests, it was found that the lower limits of detectable concentrations were 25 parts per million (ppm) for hydrogen, 100 ppm for helium, slightly higher than 25 ppm for oxygen, and slightly higher than 10 ppm for argon.

This work was done by William Helms of **Kennedy Space Center**; *Timothy P. Griffin of Dynacs, Inc.; and Andrew Ottens and Willard Harrison of the University of Florida. Further information is contained in a TSP (see page 1). KSC-12428*

Miniature Laser Doppler Velocimeter for Measuring Wall Shear
Interference fringes are configured for sensitivity to a velocity gradient.

NASA's Jet Propulsion Laboratory, Pasadena, California

A miniature optoelectronic instrument has been invented as a nonintrusive means of measuring a velocity gradient proportional to a shear stress in a flow near a wall. The instrument, which can be mounted flush with the wall, is a variant of a basic laser Doppler velocimeter. The laser Doppler probe volume can be located close enough to the wall (as little as 100 μm from the surface) to lie within the viscosity-dominated sublayer of a turbulent boundary layer.

A **Unitary Assembly of Optical Components** is fabricated on a quartz substrate. For the sake of simplicity, such non-optical details as alignment marks and mounting features are omitted from this view.

Like other laser Doppler velocimeters, this instrument includes optics that split a laser beam into two parts that impinge on the probe volume from two different directions to form interference fringes in the probe volume. Also like other laser Doppler velocimeters, this instrument measures the frequency of variation of light reflected by particles entrained in the flow as they pass through the fringes (the velocity component that one seeks to measure is simply the product of this frequency and the fringe spacing). What distinguishes this instrument from other laser Doppler velocimeters is its highly miniaturized design and its unique fringe geometry.

The instrument (see figure) includes a diode laser, the output of which is shaped by a diffractive optical element (DOE) into two beams that have elliptical cross sections with very high aspect ratios. The DOE focuses these beams through two slits a few microns apart on a surface that, in use, is mounted flush with the wall that bounds the flow. Light reflected from flow particles that pass through the fringes is collected through a window (essentially, a third, wider slit). Another DOE acts as focusing lens that couples the collected light into an opti-cal fiber that, in turn, couples the light to an avalanche photodiode. The output of the photodiode is processed to measure the frequency of variation in the intensity of the reflected light.

The interference between the laser beams forms fringes that diverge by an amount proportional to the distance from the wall: the fringes appear as radial spokes in the plane that contains a parallel-to-the-wall velocity component to be measured. Because the magnitude of this velocity component also increases linearly with distance from the wall in the viscosity-dominated flow regime and because the corresponding component of shear stress is proportional to the perpendicular-to-the-wall gradient of this velocity component, it follows that the frequency of variation of light reflected by particles entrained in the flow is proportional to the shear-stress component that one seeks to measure.

The critical optical components for manipulating the laser light are fabricated on a 0.5-mm-thick quartz substrate in a sequence of microfabrication steps. The front surface (the top surface in the figure) is coated with a thin film of chromium, then further coated with poly(methyl methacrylate) [PMMA].

The slits and window are formed in the chromium film by electron-beam lithography followed by wet etching. The back surface is coated with PMMA, in which the DOEs are formed by electron-beam lithography. The unitary assembly of optical components thus formed is mounted in a compact housing that also holds the diode laser and the fiber-optic-coupled photodiode.

Coherent Laser Instrument Would Measure Range and Velocity
This lightweight, low-power, compact instrument could have a variety of uses.

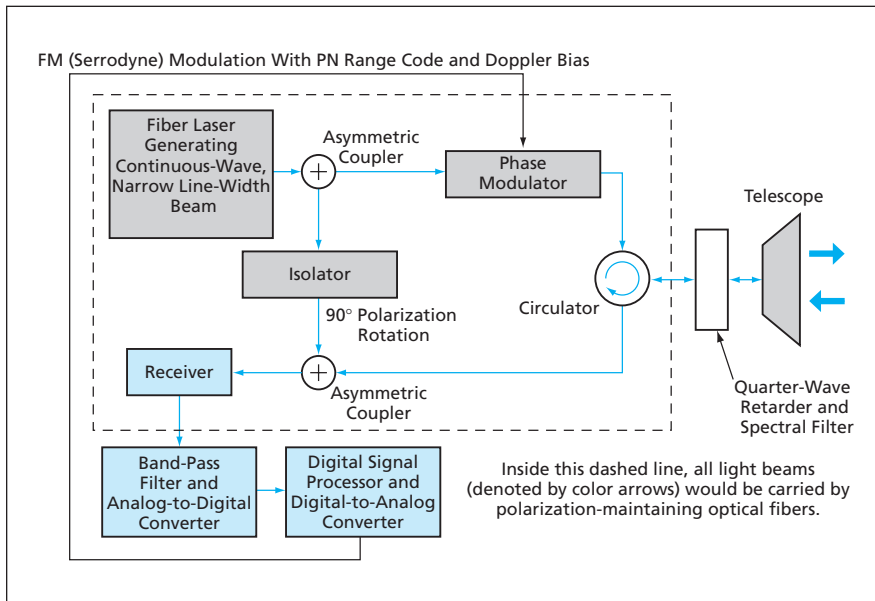*NASA's Jet Propulsion Laboratory, Pasadena, California*

A proposed instrument would project a narrow laser beam that would be frequency-modulated with a pseudo-random noise (PN) code for simultaneous measurement of range and velocity along the beam. The instrument performs these functions in a low mass, power, and volume package using a novel combination of established techniques. Originally intended as a low resource-footprint guidance sensor for descent and landing of small spacecraft onto Mars or small bodies (e.g., asteroids), the basic instrument concept also lends itself well to a similar application guiding aircraft (especially, small unmanned aircraft), and to such other applications as ranging of topographical features and measuring velocities of airborne light-scattering particles as wind indicators.

Several key features of the instrument's design contribute to its favor-able performance and resource-consumption characteristics. A laser beam is intrinsically much narrower (for the same exit aperture telescope or antenna) than a radar beam, eliminating the need to correct for the effect of sloping terrain over the beam width, as is the case with radar. Furthermore, the use of continuous-wave (CW), erbium-doped fiber lasers with excellent spectral purity (narrow line width) permits greater velocity resolution, while reducing the laser's power requirement compared to a more typical pulsed solid-state laser. The use of CW also takes proper advantage of the increased sensitivity of coherent detection, necessary in the first place for direct measurement of velocity using the Doppler effect. However, measuring range with a CW beam requires modulation to "tag" portions of it for time-of-flight determination; typically, the modulation consists of a PN code. A novel element of the instrument's design is the use of frequency modulation (FM) to accomplish both the PN-modulation and the Doppler-bias frequency shift necessary for signed velocity measurements. This permits the use of a single low-power waveguide electro-optic phase modulator, while simultaneously mitigating the effects of speckle as a noise source in the coherent detection.

The instrument (see figure) would include a narrow-line-width CW laser, the output of which would be split into a local oscillator and signal arm. Within the instrument, optical beams would be routed, split, and combined by use of fiber and planar integrated optics. The signal arm beam would be frequency-modulated by the electro-optic phase modulator, fed by a serrodyne waveform generated either in software or hard-

FM (Serrodyne) Modulation With PN Range Code and Doppler Bias

Fiber Laser Generating Continuous-Wave, Narrow Line-Width Beam

Asymmetric Coupler

Phase Modulator

Telescope

Isolator

Circulator

90° Polarization Rotation

Receiver

Asymmetric Coupler

Quarter-Wave Retarder and Spectral Filter

Band-Pass Filter and Analog-to-Digital Converter

Digital Signal Processor and Digital-to-Analog Converter

Inside this dashed line, all light beams (denoted by color arrows) would be carried by polarization-maintaining optical fibers.

The **Proposed Laser Instrument** would perform ranging and velocimetry by use of a novel combination of established techniques. Integrated and fiber optics would be used to implement much of the functionality in a compact, lightweight package.

ware, then sent through a multiplexer to a fixed-focus collimating telescope. The combination of a fiber-coupled Faraday circulator and a quarter-wave polarization retarder forms an effective transmit/receive multiplexer, as well as outputting the desired circular polarization.

The return signal, coupled back into the instrument by the same telescope, would be mixed with the local oscillator beam in a semiconductor optical receiver. The resulting heterodyne signal would be filtered, then directly digitized for processing in the digital signal processor, where frequency demodulation and PN-code correlation would be performed, with phase-edge detection and tracking for increased range accuracy.

Printed Microinductors for Flexible Substrates

Magnetic composite layers are combined with hermetic coatings to optimize electrical and mechanical properties.

NASA's Jet Propulsion Laboratory, Pasadena, California

A method of fabricating planar, flexible microinductors that exhibit a relatively high quality factor (*Q*) between 1 and 10 MHz has been devised. These inductors are targeted for use in flexible, low-profile power-converter circuits. They could also be incorporated into electronic circuits integrated into flexible structures, including flexible antenna and solar-sail structures that are deployable.

Fabrication of inductors on flexible, heat-sensitive substrates is typically limited by the need for high-temperature annealing step of the magnetic material. Highly loaded ceramic/polymer composite films can be seen printed and cured at lower temperatures, but suffer

poor adhesion. Thus, a new approach is required to enable the fabrication of high *Q* inductors (for power applications) on the flex substrates.

The microinductor comprises a planar spiral metal coil and a high-permeability magnetic thick-film (equivalent to the core of a conventional inductor) in the form of a ceramic/polymer composite. The metal spiral is fabricated by photolithography and etching of a copper-clad flexible polyamide substrate. The ceramic/polymer composite is deposited by stencil and screen printing, both above and below the metal spiral (see figure).

To obtain sufficient permeance and volume magnetization for the required degree of enhancement of inductance, the mass fraction of the ceramic in the ceramic/polymer composite must be about 95 percent, which is greater than the mass fractions of fillers typically incorporated into polymer-matrix thick films. In general, such a high mass fraction of filler can adversely affect printability and adhesion and can make the printed thick films susceptible to mechanical failure and

delamination during flexure. These adverse effects can be overcome, to a degree that makes it possible to produce an inductor of both acceptably high *Q* and acceptable mechanical properties, by (1) proper choice of the polymer resin and the ceramic magnetic powder filler for the thick-film formulation, in conjunction with (2) the use of a hermetic-coating technique.

Of the resins tested, polyester resins demonstrated the best loading and adhesion characteristics. A magnetic powder comprising Mn-Zn ferrite particles about 10 μm in diameter was found to yield good magnetic properties. It was found that improved adhesion could be obtained through coating with vacuum-polymerized parylene.

This work was done by Erik Brandon, Jay Whitacre, and Emily Wesseling of Caltech for **NASA's Jet Propulsion Laboratory.** *Further information is contained in a TSP (see page 1).*
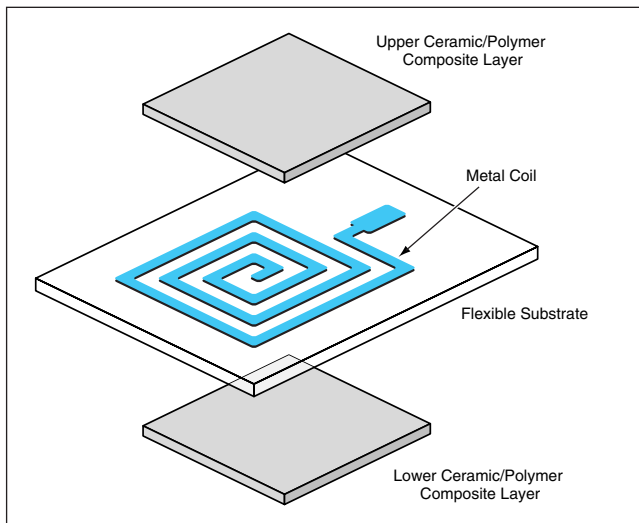
A **Flexible Inductor of Three Layers** is fabricated as an integral unit by thick-film processing techniques.

Labels in figure: Upper Ceramic/Polymer Composite Layer; Metal Coil; Flexible Substrate; Lower Ceramic/Polymer Composite Layer

Series-Connected Buck Boost Regulators

Sizes and power losses are smaller than those of conventional switching voltage regulators.

John H. Glenn Research Center, Cleveland, Ohio

A series-connected buck boost regulator (SCBBR) is an electronic circuit that bucks a power-supply voltage to a lower regulated value or boosts it to a higher regulated value. The concept of the SCBBR is a generalization of the con-

cept of the SCBR, which was reported in "Series-Connected Boost Regulators" (LEW-15918), *NASA Tech Briefs*, Vol. 23, No. 7 (July 1997), page 42. Relative to prior DC-voltage-regulator concepts, the SCBBR concept can yield significant re-

ductions in weight and increases in power-conversion efficiency in many applications in which input/output voltage ratios are relatively small and isolation is not required, as solar-array regulation or battery charging with DC-bus regulation.
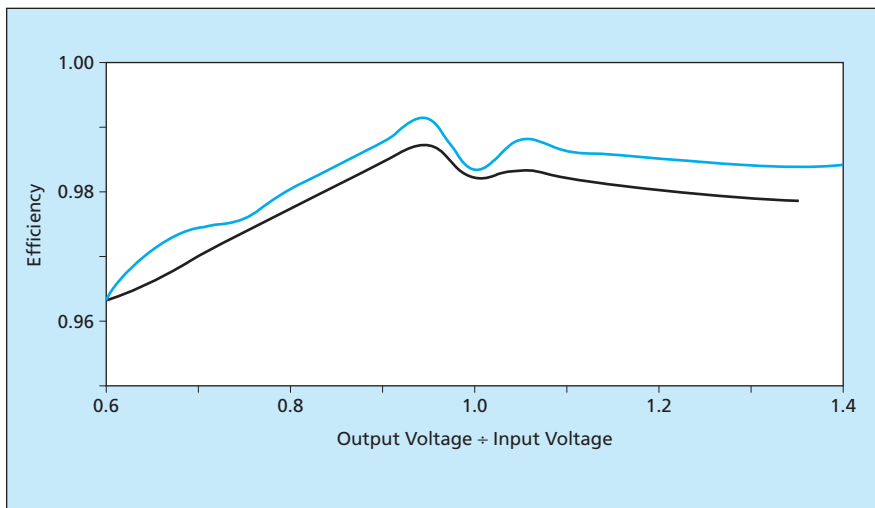
Figure 1. **The Efficiency of a Breadboard SCBBR** was measured as a function of output voltage with input voltage held at 120 V. (The upper curve is for a 5-A load; the lower is for a 2-A load.)
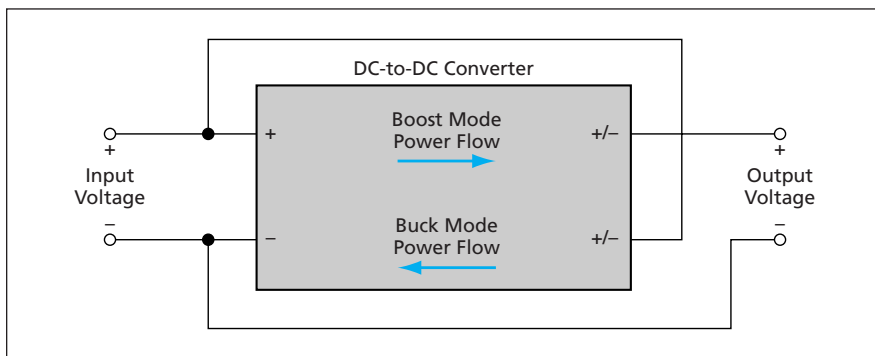

Figure 2. In a **Basic SCBBR**, the input side of a DC-to-DC converter is connected across the input power bus, while the output side is connected in series with the input power bus.

Usually, a DC voltage regulator is designed to include a DC-to-DC converter to reduce its power loss, size, and weight. Advances in components, increases in operating frequencies, and improved circuit topologies have led to continual increases in efficiency and/or decreases in the sizes and weights of DC voltage regulators. The primary source of inefficiency in the DC-to-DC converter portion of a voltage regulator is the conduction loss and, especially at high frequencies, the switching loss. Although improved components and topology can reduce the switching loss, the reduction is limited by the fact that the converter generally switches all the power being regulated.

Like the SCBR concept, the SCBBR concept involves a circuit configuration in which only a fraction of the power is switched, so that the switching loss is reduced by an amount that is largely independent of the specific components and circuit topology used. In an SCBBR, the amount of power switched by the DC-to-DC converter is only the amount needed to make up the difference between the input and output bus voltage. The remaining majority of the power passes through the converter without being switched.

The weight and power loss of a DC-to-DC converter are determined primarily by the amount of power processed. In the SCBBR, the unswitched majority of the power is passed through with very little power loss, and little if any increase in the sizes of the converter components is needed to enable the components to handle the unswitched power. As a result, the power-conversion efficiency of the regulator can be very high, as shown in the example of Figure 1.

A basic SCBBR includes a DC-to-DC converter (see Figure 2). The switches and primary winding of a transformer in the converter is connected across the input bus, while the secondary winding and switches are connected in series with the output bus, so that the output voltage is the sum of the input voltage and the secondary voltage of the converter.

In the breadboard SCBBR, the input voltage applied to the primary winding is switched by use of metal oxide/semi-conductor field-effect transistors (MOSFETs) in a full bridge circuit; the secondary winding is center-tapped, with two MOSFET switches and diode rectifiers connected in opposed series in each leg. The sets of opposed switches and rectifiers are what enable operation in either a boost or a buck mode. In the boost mode, input voltage and current, and the output voltage and current are all positive; that is, the secondary voltage is added to the input voltage and the net output voltage can be regulated at a value equal or greater than the input voltage. In the buck mode, input voltage is still positive and the current still flows in the same direction in the secondary, but the switches are controlled such that some power flows from the secondary to the primary. The voltage across the secondary and the current into the primary are reversed. The result is that the output voltage is lower than the input voltage, and some power is recirculated from the converter secondary back to the input.

Quantitatively, the advantage of an SCBBR is a direct function of the regulation range required. If, for example, a regulation range of ±20 percent is required for a 500-W supply, then it suffices to design the DC-to-DC converter in the SCBBR for a power rating of only 100 W. The switching loss and size are much smaller than those of a conventional regulator that must be rated for switching of all 500 W. The reduction in size and the increase in efficiency are not directly proportional to switched-power ratio of 5:1 because the additional switches contribute some conduction loss and the input and output filters must be larger than those typically required for a 100-W converter. Nevertheless, the power loss and the size can be much smaller than those of a 500-W converter.

Because with slight additions the SCBBR can also function as a conventional buck-mode switching regulator, it can provide current-limited turn-on, protection against overcurrent, and bus switching. Finally, it should be noted that although the breadboard SCBBR design utilizes hard switching, resonant and soft-switching configurations should be viable as alternatives.
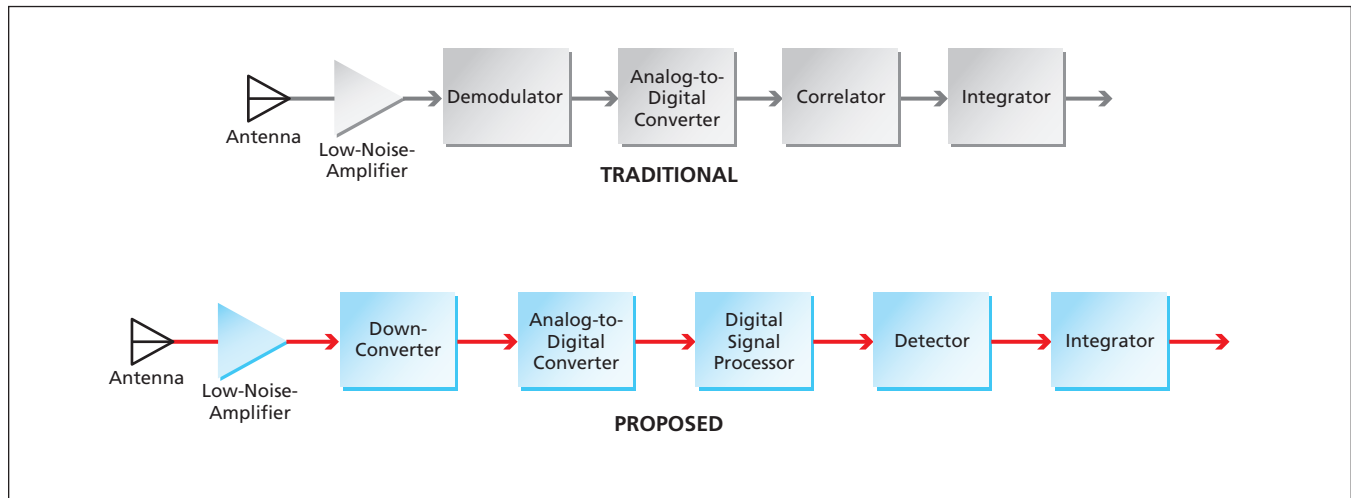
Digital Receiver for Microwave Radiometry

Interfering signals would be suppressed in digital signal processing.

Goddard Space Flight Center, Greenbelt, Maryland

The **Proposed Microwave Radiometer Receiver** would include a digital signal processor that would execute interference-suppression algorithms.

A receiver proposed for use in L-band microwave radiometry (for measuring soil moisture and sea salinity) would utilize digital signal processing to suppress interfering signals. Heretofore, radio-frequency interference has made it necessary to limit such radiometry to a frequency band about 20 MHz wide, centered at ≈1,413 MHz. The suppression of interference in the proposed receiver would make it possible to expand the frequency band to a width of 100 MHz, thereby making it possible to obtain greater sensitivity and accuracy in measuring moisture and salinity.

The receiver would digitize a portion of the received signal spectrum up to 100 MHz wide. The digitized signals would be processed to extract either the total power or the power spectral density associated with the physical processes of interest. The processing would involve the use of adaptive and parametric filtering techniques implemented in real time by use of reconfigurable digital hardware in the form of field-programmable gate arrays.

The microwave signals emitted by the physical processes of interest are quasi-stationary and noiselike. The signal-processing algorithms would include interference-suppression algorithms, which would be based partly on the assumption that signals that are not both quasi-stationary and noiselike must be interfering signals. For example, pulses would be detected and blanked. Following blanking of pulse and other suppression of interfering signals, a fast Fourier transform (FFT) would be applied. The FFT outputs would be integrated, and the results of the integrations would be transferred to a computer for storage.

This work was done by Steven W. Ellingson, Grant A. Hampson, and Joel T. Johnson of Ohio State University for **Goddard Space Flight Center**. *Further information is contained in a TSP (see page 1).*
GSC-14776-1

Printed Antennas Made Reconfigurable by Use of MEMS Switches

MEMS switches offer advantages over electronic control circuits.

John H. Glenn Research Center, Cleveland, Ohio

A class of reconfigurable microwave antennas now undergoing development comprise fairly conventional printed-circuit feed elements and radiating patches integrated with novel switches containing actuators of the micro-electromechanical systems (MEMS) type. In comparison with solid-state electronic control devices incorporated into some prior printed microwave an-

tennas, the MEMS-based switches in these antennas impose lower insertion losses and consume less power. Because the radio-frequency responses of the MEMS switches are more nearly linear, they introduce less signal distortion. In addition, construction and operation are simplified because only a single DC bias line is needed to control each MEMS actuator.

The incorporation of the MEMS switches makes it possible for an antenna of this class to operate over several frequency bands without undergoing changes in its dimensions other than the small deflections associated with opening and closing gaps between switch contacts. In addition, the polarization of the radiation emitted or received by the antenna can be

FREQUENCY-SWITCHABLE ANTENNA CONTAINING MEMS ACTUATORS

$L = 580 \ \mu m \quad a = 2.6 \ mm$
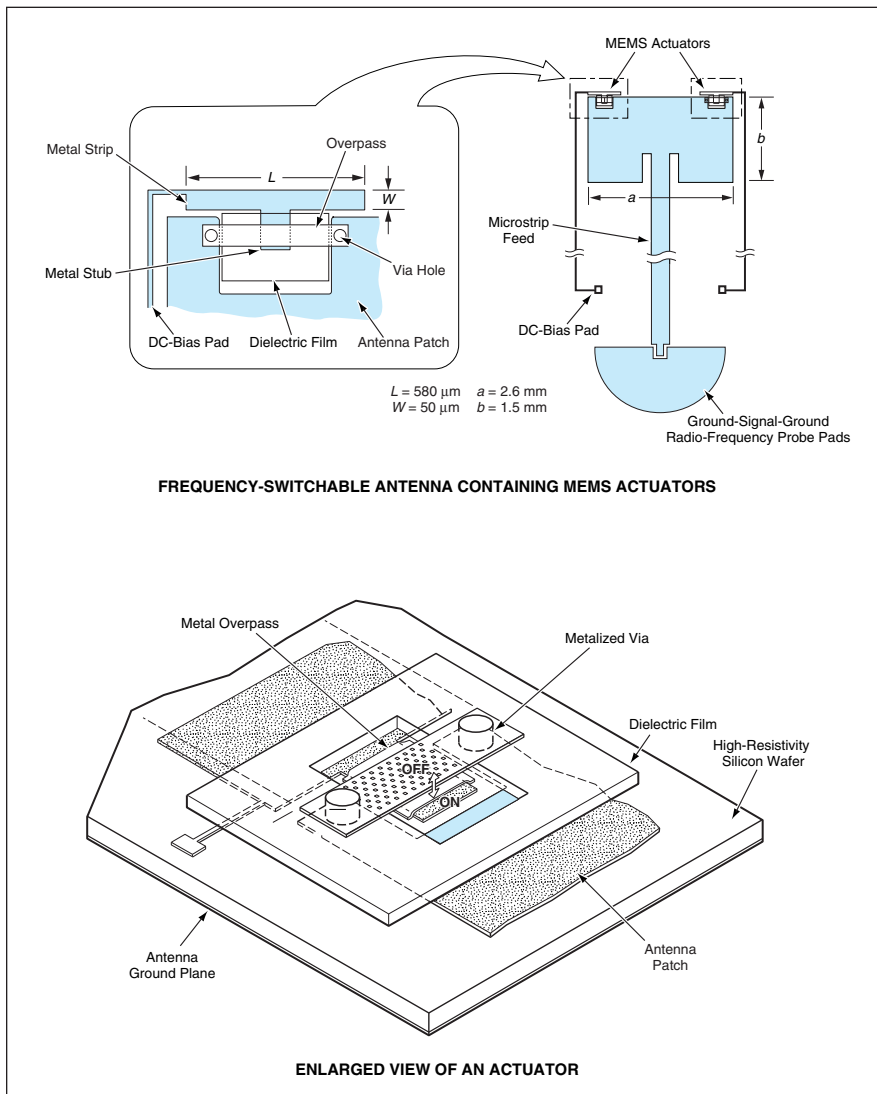$W = 50 \ \mu m \quad b = 1.5 \ mm$

ENLARGED VIEW OF AN ACTUATOR

Figure 1. The **Two Independent MEMS Actuators** in this patch antenna can be used to change the operating frequency. When both actuators are off, the frequency is about 25.0 GHz. When one of the actuators is on, the frequency is 24.8 GHz. When both actuators are on, the frequency is 24.6 GHz.
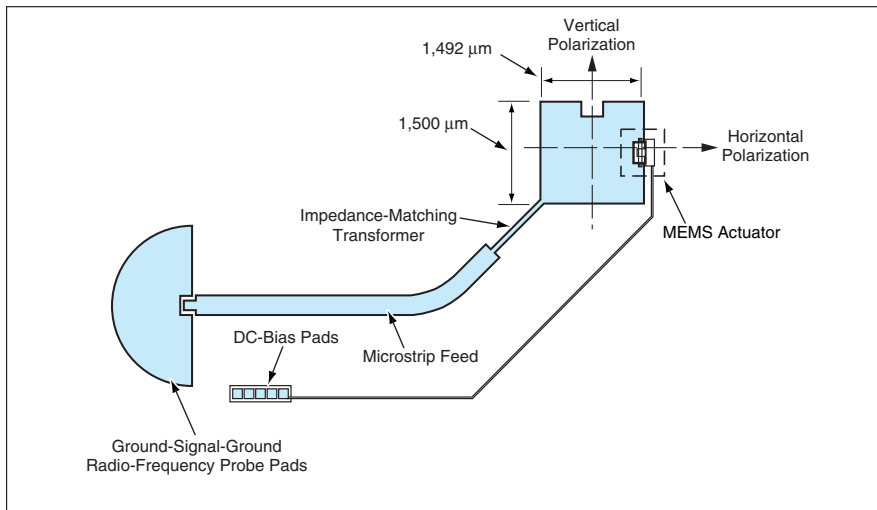

Figure 2. This **Patch Antenna** radiates in circular polarization when the actuator is off and in dual linear polarization when the actuator is on.

switched between linear and circular. The ability to change frequency and polarization makes these antennas attractive for inclusion in planar phased antenna arrays.

The upper part of Figure 1 shows the layout of one such antenna containing two MEMS actuators, while the lower part of this figure presents an enlarged view of one of the actuators. Each actuator includes a flexible metal overpass suspended over a metal stub. The overpass is supported at its ends by metal vias electrically connected to the antenna patch. A dielectric film occupies part of the gap between the stub and the overpass. The overpass is free to bend up and down and is actuated in bending by electrostatic attraction by a DC bias voltage applied between the overpass and the metal stub. A metal strip of length L and width W attached to metal stub behaves as a parallel-plate capacitor.

When an actuator is in the "off" state (voltage not applied, overpass not bent), the antenna patch operates at a nominal frequency determined by the dimension b. When the actuator is in the "on" state (voltage applied, overpass bent down), the capacitance of the metal strip appears in shunt with the input impedance of the antenna patch. This capacitance tunes the antenna to a lower operating frequency. During the design-synthesis process, the inductances and capacitances of the actuators and their locations in the patch should be taken into account in order to ensure constant input impedance.

The antenna depicted in Figure 2 is designed to support two degenerate orthogonal modes when excited at a corner. When the MEMS actuator in this antenna is in the "off" state, the perturbation of the modes is negligible and the patch radiates a circularly polarized wave. When the actuator is in the "on" state, the phase relation between the two modes is perturbed to a degree that causes the patch to radiate dual linearly polarized waves.

This work was done by Rainee N. Simons of **Glenn Research Center**. *Further information is contained in a TSP (see page 1).*

Inquiries concerning rights for the commercial use of this invention should be addressed to NASA Glenn Research Center, Commercial Technology Office, Attn: Steve Fedor, Mail Stop 4-8, 21000 Brookpark Road, Cleveland Ohio 44135. Refer to LEW-17389.

Software

Traffic-Light-Preemption Vehicle-Transponder Software Module

A prototype wireless data-communication and control system automatically modifies the switching of traffic lights to give priority to emergency vehicles. The system, which was reported in several *NASA Tech Briefs* articles at earlier stages of development, includes a transponder on each emergency vehicle, a monitoring and control unit (an intersection controller) at each intersection equipped with traffic lights, and a central monitoring subsystem. An essential component of the system is a software module executed by a microcontroller in each transponder. This module integrates and broadcasts data on the position, velocity, acceleration, and emergency status of the vehicle. The position, velocity, and acceleration data are derived partly from the Global Positioning System, partly from deductive reckoning, and partly from a diagnostic computer aboard the vehicle. The software module also monitors similar broadcasts from other vehicles and from intersection controllers, informs the driver of which intersections it controls, and generates visible and audible alerts to inform the driver of any other emergency vehicles that are close enough to create a potential hazard. The execution of the software module can be monitored remotely and the module can be upgraded remotely and, hence, automatically.

*This program was written by Aaron Bachelder and Conrad Foster of Caltech for **NASA's Jet Propulsion Laboratory**. Further information is contained in a TSP (see page 1).*

This software is available for commercial licensing. Please contact Don Hart of the California Institute of Technology at (818) 393-3425. Refer to NPO-30445.

Intersection-Controller Software Module

An important part of the emergency-vehicle traffic-light-preemption system summarized in the preceding article is a software module executed by a microcontroller in each intersection controller. This module monitors the broadcasts from all nearby participating emergency vehicles and intersections. It gathers the broadcast data pertaining to the positions and velocities of the vehicles and the timing of traffic and pedestrian lights and processes the data into predictions of the future positions of the vehicles. Analyzing the predictions by a combination of proximity tests, map-matching techniques, and statistical calculations designed to minimize the adverse effects of uncertainties in vehicle positions and headings, the module decides whether to preempt and issues the appropriate commands to the traffic lights, pedestrian lights, and electronic warning signs at the intersection. The module also broadcasts its state to all nearby vehicles and intersections. The module is designed to mitigate the effects of missing data and of unpredictable delays in the system. It has been intensively tested and refined so that it fails to warn in very few cases and issues very few false warnings.

*This program was written by Aaron Bachelder and Conrad Foster of Caltech for **NASA's Jet Propulsion Laboratory**. Further information is contained in a TSP (see page 1).*

This software is available for commercial licensing. Please contact Don Hart of the California Institute of Technology at (818) 393-3425. Refer to NPO-30446.

Central-Monitor Software Module

One of the software modules of the emergency-vehicle traffic-light-preemption system of the two preceding articles performs numerous functions for the central monitoring subsystem. This module monitors the states of all units (vehicle transponders and intersection controllers): It provides real-time access to the phases of traffic and pedestrian lights, and maps the positions and states of all emergency vehicles. Most of this module is used for installation and configuration of units as they are added to the system. The module logs all activity in the system, thereby providing information that can be analyzed to minimize response times and optimize response strategies. The module can be used from any location within communication range of the system; with proper configuration, it can also be used via the Internet. It can be integrated into call-response centers, where it can be used for alerting emergency vehicles and managing their responses to specific incidents. A variety of utility subprograms provide access to any or all units for purposes of monitoring, testing, and modification. Included are "sniffer" utility subprograms that monitor incoming and outgoing data for accuracy and timeliness, and that quickly and autonomously shut off malfunctioning vehicle or intersection units.

*This program was written by Aaron Bachelder and Conrad Foster of Caltech for **NASA's Jet Propulsion Laboratory**. Further information is contained in a TSP (see page 1).*

This software is available for commercial licensing. Please contact Don Hart of the California Institute of Technology at (818) 393-3425. Refer to NPO-30447.

Estimating Effects of Multi-path Propagation on GPS Signals

Multipath Simulator Taking into Account Reflection and Diffraction (MUSTARD) is a computer program that simulates effects of multipath propagation on received Global Positioning System (GPS) signals. MUSTARD is a very efficient means of estimating multipath-induced position and phase errors as functions of time, given the positions and orientations of GPS satellites, the GPS receiver, and any structures near the receiver as functions of time. MUSTARD traces each signal from a GPS satellite to the receiver, accounting for all possible paths the signal can take, including all paths that include reflection and/or diffraction from surfaces of structures near the receiver and on the satellite. Reflection and diffraction are modeled by use of the geometrical theory of diffraction. The multipath signals are added to the direct signal after accounting for the gain of the receiving antenna. Then, in a simulation of a delay-lock tracking loop in the receiver, the multipath-induced range and phase errors as measured by the receiver are estimated. All of these computations are performed for both right circular polarization and left circular polarization of

both the L1 (1.57542-GHz) and L2 (1.2276-GHz) GPS signals.

This program was written by Sung Byun, George Hajj, and Lawrence Young of Caltech for **NASA's Jet Propulsion Laboratory**. *Further information is contained in a TSP (see page 1)..*

This software is available for commercial licensing. Please contact Don Hart of the California Institute of Technology at (818) 393-3425. Refer to NPO-40463.

Parallel Adaptive Mesh Refinement Library

Parallel Adaptive Mesh Refinement Library (PARAMESH) is a package of Fortran 90 subroutines designed to provide a computer programmer with an easy route to extension of (1) a previously written serial code that uses a logically Cartesian structured mesh into (2) a parallel code with adaptive mesh refinement (AMR). Alternatively, in its simplest use, and with minimal effort, PARAMESH can operate as a domain-decomposition tool for users who want to parallelize their serial codes but who do not wish to utilize adaptivity. The package builds a hierarchy of sub-grids to cover the computational domain of a given application program, with spatial resolution varying to satisfy the demands of the application. The sub-grid blocks form the nodes of a tree data structure (a quad-tree in two or an oct-tree in three dimensions). Each grid block has a logically Cartesian mesh. The package supports one-, two- and three-dimensional models.

This program was written by Peter MacNeice of Raytheon/STX and Kevin Olson of George Mason University for **Goddard Space Flight Center**. *For further information, access http://sdcd.gsfc.nasa.gov/RIB/repositories/inhouse_gsfc/Users_manual/amr_tutorial.html. GSC-14626-1*

Space Physics Data Facility Web Services

The Space Physics Data Facility (SPDF) Web services provides a distributed programming interface to a portion of the SPDF software. (A general description of Web services is available at *http://www.w3.org/* and in many current software-engineering texts and articles focused on distributed programming.) The SPDF Web services distributed programming interface enables additional collaboration and integration of the SPDF software system with other software systems, in furtherance of the SPDF mission to lead collaborative efforts in the collection and utilization of space physics data and mathematical models. This programming interface conforms to all applicable Web services specifications of the World Wide Web Consortium. The interface is specified by a Web Services Description Language (WSDL) file. The SPDF Web services software consists of the following components:
- A server program for implementation of the Web services; and
- A software developer's kit that consists of a WSDL file, a less formal description of the interface, a Java class library (which further eases development of Java-based client software), and Java source code for an example client program that illustrates the use of the interface.

This program was written by Robert M. Candey, Bernard T. Harris, and Reine A. Chimiak of **Goddard Space Flight Center**. *For further information, access http://spdf.gsfc.nasa.gov/. GSC-14730-1*

Predicting Noise From Aircraft Turbine-Engine Combustors

COMBUSTOR and CNOISE are computer codes that predict far-field noise that originates in the combustors of modern aircraft turbine engines — especially modern, low-gaseous-emission engines, the combustors of which sometimes generate several decibels more noise than do the combustors of older turbine engines. COMBUSTOR implements an empirical model of combustor noise derived from correlations between engine-noise data and operational and geometric parameters, and was developed from databases of measurements of acoustic emissions of engines. CNOISE implements an analytical and computational model of the propagation of combustor temperature fluctuations (hot spots) through downstream turbine stages. Such hot spots are known to give rise to far-field noise. CNOISE is expected to be helpful in determining why low-emission combustors are sometimes noisier than older ones, to provide guidance for refining the empirical correlation model embodied in the COMBUSTOR code, and to provide insight on how to vary downstream turbine-stage geometry to reduce the contribution of hot spots to far-field noise.

These programs were written by P. Gliebe, R. Mani, S. Salamah, and R. Coffin of General Electric Co. and Jayesh Mehta of Diversitec, Inc., for **Glenn Research Center**. *Further information is contained in a TSP (see page 1).*

Inquiries concerning rights for the commercial use of this invention should be addressed to NASA Glenn Research Center, Commercial Technology Office, Attn: Steve Fedor, Mail Stop 4-8, 21000 Brookpark Road, Cleveland, Ohio 44135. Refer to LEW-17385-1.

Generating Animated Displays of Spacecraft Orbits

Tool for Interactive Plotting, Sonification, and 3D Orbit Display (TIPSOD) is a computer program for generating interactive, animated, four-dimensional (space and time) displays of spacecraft orbits. TIPSOD utilizes the programming interface of the Satellite Situation Center Web (SSCWeb) services to communicate with the SSC logic and database by use of the open protocols of the Internet. TIPSOD is implemented in Java 3D and effects an extension of the pre-existing SSCWeb two-dimensional static graphical displays of orbits. Orbits can be displayed in any or all of the following seven reference systems: true-of-date (an inertial system), J2000 (another inertial system), geographic, geomagnetic, geocentric solar ecliptic, geocentric solar magnetospheric, and solar magnetic. In addition to orbits, TIPSOD computes and displays Sibeck's magnetopause and Fairfield's bow-shock surfaces. TIPSOD can be used by the scientific community as a means of projection or interpretation. It also has potential as an educational tool. Documentation and links for downloading the software can be found at *http://sscweb.gsfc.gov/tipsod/*.

This program was written by Robert M. Candey, Reine A. Chimiak, and Bernard T. Harris of **Goddard Space Flight Center**. *For more information contact the Goddard Commercial Technology Office at (301) 286-5810. GSC-14732-1*

Diagnosis and Prognosis of Weapon Systems

The Prognostics Framework is a set of software tools with an open architecture that affords a capability to integrate various prognostic software mechanisms and to provide information for operational and battlefield decision-making and logistical planning pertaining to weapon systems. The Prognostics

Framework is also a system-level "health"-management software system that (1) receives data from performance-monitoring and built-in-test sensors and from other prognostic software and (2) processes the received data to derive a diagnosis and a prognosis for a weapon system. This software relates the diagnostic and prognostic information to the overall health of the system, to the ability of the system to perform specific missions, and to needed maintenance actions and maintenance resources. In the development of the Prognostics Framework, effort was focused primarily on extending previously developed model-based diagnostic-reasoning software to add prognostic reasoning capabilities, including capabilities to perform statistical analyses and to utilize information pertaining to deterioration of parts, failure modes, time sensitivity of measured values, mission criticality, historical data, and trends in measurement data. As thus extended, the software offers an overall health-monitoring capability.

This program was written by Mary Nolan, Rebecca Catania, and Gregory deMare of Giordano Automation Corp. for **Marshall Space Flight Center**. *Further information is contained in a TSP (see page 1).*
MFS-31644

⊘ Training Software in Artificial-Intelligence Computing Techniques

The Artificial Intelligence (AI) Toolkit is a computer program for training scientists, engineers, and university students in three soft-computing techniques (fuzzy logic, neural networks, and genetic algorithms) used in artificial-intelligence applications. The program promotes an easily understandable tutorial interface, including an interactive graphical component through which the user can gain hands-on experience in soft-computing techniques applied to realistic example problems. The tutorial provides step-by-step instructions on the workings of soft-computing technology, whereas the hands-on examples allow interaction and reinforcement of the techniques explained throughout the tutorial. In the fuzzy-logic example, a user can interact with a robot and an obstacle course to verify how fuzzy logic is used to command a rover traverse from an arbitrary start to the goal location. For the genetic algorithm example, the problem is to determine the minimum-length path for visit-

ing a user-chosen set of planets in the solar system. For the neural-network example, the problem is to decide, on the basis of input data on physical characteristics, whether a person is a man, woman, or child. The AI Toolkit is compatible with the Windows 95,98, ME, NT 4.0, 2000, and XP operating systems. A computer having a processor speed of at least 300 MHz, and random-access memory of at least 56MB is recommended for optimal performance. The program can be run on a slower computer having less memory, but some functions may not be executed properly.

This program was written by Ayanna Howard, Eric Rogstad, and Eugene Chalfant of Caltech for **NASA's Jet Propulsion Laboratory**. *Further information is contained in a TSP (see page 1).*

This software is available for commercial licensing. Please contact Don Hart of the California Institute of Technology at (818) 393-3425. Refer to NPO-40496.

⊘ APGEN Version 5.0

Activity Plan Generator (APGEN), now at version 5.0, is a computer program that assists in generating an integrated plan of activities for a spacecraft mission that does not oversubscribe spacecraft and ground resources. APGEN generates an interactive display, through which the user can easily create or modify the plan. The display summarizes the plan by means of a time line, whereon each activity is represented by a bar stretched between its beginning and ending times. Activities can be added, deleted, and modified via simple mouse and keyboard actions. The use of resources can be viewed on resource graphs. Resource and activity constraints can be checked. Types of activities, resources, and constraints are defined by simple text files, which the user can modify. In one of two modes of operation, APGEN acts as a planning expert assistant, displaying the plan and identifying problems in the plan. The user is in charge of creating and modifying the plan. In the other mode, APGEN automatically creates a plan that does not oversubscribe resources. The user can then manually modify the plan. APGEN is designed to interact with other software that generates sequences of timed commands for implementing details of planned activities.

This program was written by Pierre Maldague, Dennis Page, and Adam Chase of Caltech for **NASA's Jet Propulsion Laboratory**. *Further information is contained in a TSP (see page 1).*

This software is available for commercial

licensing. Please contact Don Hart of the California Institute of Technology at (818) 393-3425. Refer to NPO-40520.

⊘ Single-Command Approach and Instrument Placement by a Robot on a Target

AUTOAPPROACH is a computer program that enables a mobile robot to approach a target autonomously, starting from a distance of as much as 10 m, in response to a single command. AUTOAPPROACH is used in conjunction with (1) software that analyzes images acquired by stereoscopic cameras aboard the robot and (2) navigation and path-planning software that utilizes odometer readings along with the output of the image-analysis software. Intended originally for application to an instrumented, wheeled robot (rover) in scientific exploration of Mars, AUTOAPPROACH could be adapted to terrestrial applications, notably including the robotic removal of land mines and other unexploded ordnance. A human operator generates the approach command by selecting the target in images acquired by the robot cameras. The approach path consists of multiple legs. Feature points are derived from images that contain the target and are thereafter tracked to correct odometric errors and iteratively refine estimates of the position and orientation of the robot relative to the target on successive legs. The approach is terminated when the robot attains the position and orientation required for placing a scientific instrument at the target. The workspace of the robot arm is then autonomously checked for self/terrain collisions prior to the deployment of the scientific instrument onto the target.

This program was written by Terrance Huntsberger and Yang Cheng of **NASA's Jet Propulsion Laboratory**. *Further information is contained in a TSP (see page 1).*

This software is available for commercial licensing. Please contact Don Hart of the California Institute of Technology at (818) 393-3425. Refer to NPO-30529

⊘ Three-Dimensional Audio Client Library

The Three-Dimensional Audio Client Library (3DAudio library) is a group of software routines written to facilitate development of both stand-alone (audio only) and immersive virtual-reality application pro-

grams that utilize three-dimensional audio displays. The library is intended to enable the development of three-dimensional audio client application programs by use of a code base common to multiple audio server computers. The 3DAudio library calls vendor-specific audio client libraries and currently supports the AuSIM Gold-Server and Lake Huron audio servers.

3DAudio library routines contain common functions for (1) initiation and termination of a client/audio server session, (2) configuration-file input, (3) positioning functions, (4) coordinate transformations, (5) audio transport functions, (6) rendering functions, (7) debugging functions, and (8) event-list-sequencing functions. The 3DAudio software is written in the C++

programming language and currently operates under the Linux, IRIX, and Windows operating systems.

This program was written by Stephen A. Rizzi of **Langley** **Research** **Center**. *For further information, contact the Intellectual Property Team at (757) 864-3521. LAR-16690-1*

Isogrid Membranes for Precise, Singly Curved Reflectors

Reinforcing meshes of fibers would prevent wrinkles and ripples.

NASA's Jet Propulsion Laboratory, Pasadena, California

A new type of composite material has been proposed for membranes that would constitute the reflective surfaces of planned lightweight, single-curvature (e.g., parabolic cylindrical) reflectors for some radar and radio-communication systems. The proposed composite materials would consist of polyimide membranes containing embedded grids of high-strength (e.g., carbon) fibers. The purpose of the fiber reinforcements, as explained in more detail below, is to prevent wrinkling or rippling of the membrane.

A membrane single-curvature reflector is made by stretching a reflective membrane between frame ends that define the specified curvature (see Figure 1). The stretching is necessary to impart the stiffness needed to maintain the required curvature. Unavoidably, the stretching also induces a negative (compressive) strain, proportional to the Poisson's ratio of the membrane material, in the direction perpendicular to the stretch direction (see Figure 2). The negative strain gives rise to wrinkles and/or ripples. In the case of a precise radar or radio-communication reflector, the degradation of performance by ripples or wrinkles would be unacceptable.

In a membrane according to the proposal, the embedded reinforcing fibers would be meshed in an isogrid pattern. The design parameters of the fibers and the pattern would be chosen so that the fibers would carry much of the stretching load in such a manner as to reduce or eliminate the compressive strains in the directions perpendicular to stretching. From a macroscopic perspective, the reduction of compressive strains could be characterized by a corresponding reduction in the effective Poisson's ratio.

As a preliminary test of the proposal, computational simulations of effects of stretching were performed for two membranes, denoted the plain and isogrid membranes. The plain membrane was made of 2-mil (≈0.05-mm)-thick polyimide, without reinforcing fibers. The isogrid membrane was identical to the plain membrane except that it contained an embedded mesh of high-modulus-of-elasticity carbon fibers. In the simulations, the
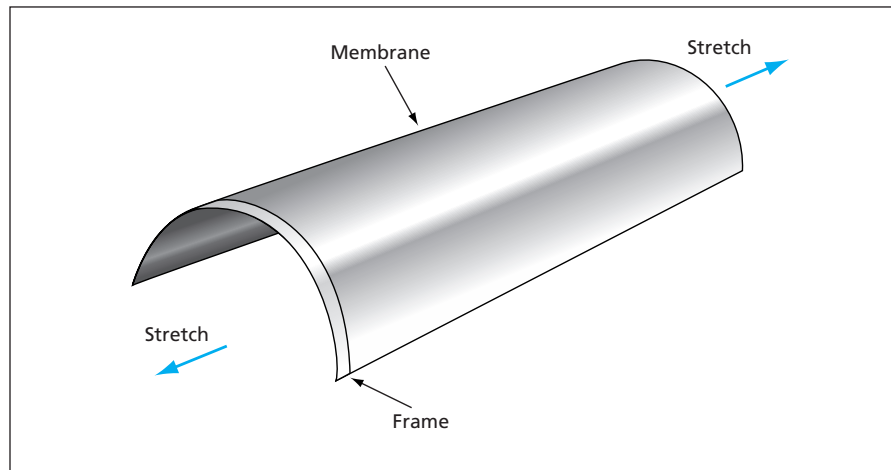

Figure 1. A **Membrane Is Stretched** between frame ends to make a lightweight, single-curvature reflector.
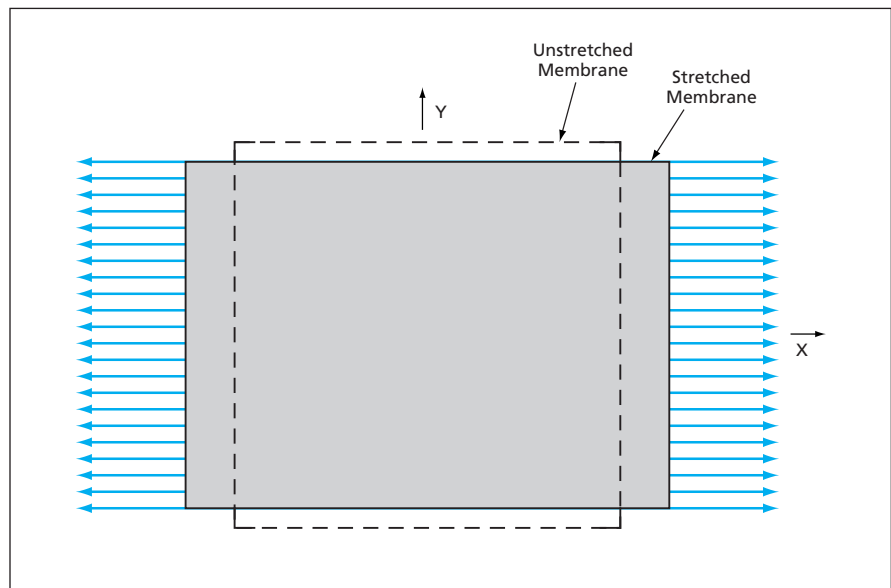

Figure 2. A **Membrane Stretched in the X Direction** contracts in the Y direction. The ratio between the Y contraction and the X stretch is denoted the Poisson's ratio of the membrane material.

membranes were stretched along one direction and their contractions along a direction perpendicular to the stretching direction were observed. For the plain membrane, the contraction perpendicular to the stretching direction was 0.33 times the stretch: in other words, the effective Poisson's ratio was 0.33, which is typical of commercially available membrane materials. For the isogrid membrane, the effective Poisson's ratio was

found to be 0.05. Further study will be necessary to determine whether this much reduction in the effective Poisson's ratio is sufficient to prevent wrinkles and ripples and whether further reductions in the effective Poisson's ratio can be achieved.

This work was done by Houfei Fang and Michael Lou of Caltech for **NASA's Jet Propulsion Laboratory**. *Further information is contained in a TSP (see page 1).*
NPO-40035

Nickel-Tin Electrode Materials for Nonaqueous Li-Ion Cells

Capacity densities exceed those of materials now commercially available for the same purpose.

Lyndon B. Johnson Space Center, Houston, Texas

Experimental materials made from mixtures of nickel and tin powders have shown promise for use as the negative electrodes of rechargeable lithium-ion electrochemical power cells. During charging (or discharging) of a lithium-ion cell, lithium ions are absorbed into (or desorbed from, respectively) the negative electrode, typically through an intercalation or alloying process. The negative electrodes (for this purpose, designated as anodes) in state-of-the-art Li-ion cells are made of graphite, in which intercalation occurs. Alternatively, the anodes can be made from metals, in which alloying can occur. For reasons having to do with the electrochemical potential of intercalated lithium, metallic anode materials (especially materials containing tin) are regarded as safer than graphite ones; in addition, such metallic anode materials have been investigated in the hope of obtaining reversible charge/discharge capacities greater than those of graphite anodes. However, until now, each of the tin-containing metallic anode formulations tested has been found to be inadequate in some respect.

In preparation for making experimental electrodes, Ni and Sn powders were mixed in various proportions and suspended in a solution of [poly(vinylidene fluoride)-hexafluoropropylene dissolved in 1-methyl-2-pyrrolidinone]. (A carbon powder was also incorporated into some of the suspensions, but subsequent tests revealed that better electrode performances were obtained without the carbon.) The experimental electrodes were then made by coating nickel foils with the suspensions and drying them in air.

The experimental electrodes were characterized through several tests, including cyclic charge/discharge tests in electrochemical cells of several different types that differed in their counter-electrode or positive-electrode materials. The electrolyte in each cell was a 1-M solution of $LiPF_6$ in a mixture of 1 part ethylene carbonate with 3 parts ethyl methyl carbonate. In each cell, the positive electrode was separated from the experimental electrode by a sheet of microporous polyethylene. Positive electrodes were made, variously, of the experimental electrode materials themselves or of lithium-metal, $LiNi_{1-x}Co_xO_2$, or $LiMn_2O_4$. Of the electrodes tested, the best results were obtained with those made from a mixture of 41.6 weight percent Ni powder and 58.4 weight percent Sn powder: These electrodes exhibited high specific charge/discharge capacity (>0.3 A·h/g), capacity density >2.5 A·h/mL (more than three times that of Li-ion-cell negative-electrode materials now commercially available), nearly zero capacity fade, low irreversible capacity (45 to 76 mA·h/g), and long cycle life.

Photocatalytic Coats in Glass Drinking-Water Bottles

Lyndon B. Johnson Space Center, Houston, Texas

According to a proposal, the insides of glass bottles used to store drinking water would be coated with films consisting of or containing TiO_2. In the presence of ultraviolet light, these films would help to remove bacteria, viruses, and trace organic contaminants from the water.

Material systems that contain TiO_2 have been observed to be photocatalytic and, in particular, to be photocatalytically effective for destroying organic compounds. Bacteriocidal films containing TiO_2 have been made, but, heretofore, have not been exploited for bacteriological protection of drinking water.

A glass bottle to be coated on the inside would be filled with a fluid suspension of TiO_2, then inverted. By controlling the rate of release of the suspension, one would control the thickness of the TiO_2 film deposited on the inner surface of the bottle. The bottle could then be fired to produce a stable, photocatalytically active TiO_2 film.

Coating with TiO_2 may also offer an additional advantage by impeding the dissolution of silica from the glass. TiO_2 is not toxic, and its solubility is much less than that of SiO_2.

Fast Laser Shutters With Low Vibratory Disturbances

Opposing cantilevered piezoelectric bending actuators balance each other to minimize vibration.

NASA's Jet Propulsion Laboratory, Pasadena, California

The figure shows a prototype vacuum-compatible, fast-acting, long-life shutter unit that generates very little vibratory disturbance during switching. This is one of a number of shutters designed to satisfy requirements specific to an experiment, to be performed aboard a spacecraft in flight, in which laser beams m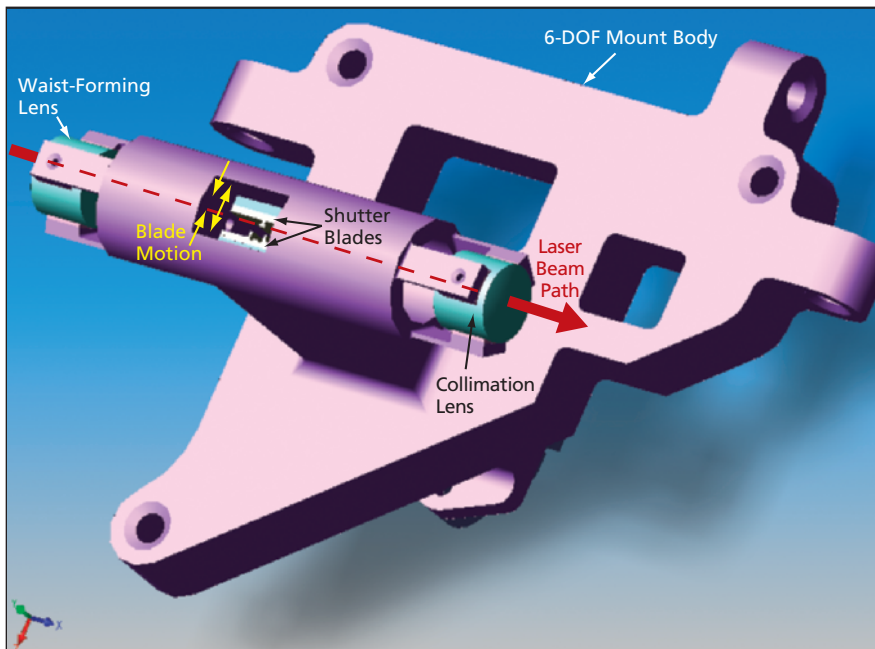ust be blocked rapidly and completely, without generating a vibratory disturbance large enough to adversely affect the power and frequency stability of the lasers. Commercial off-the-shelf laboratory shutter units — typically containing electromagnet-coil-driven mechanisms — were found not to satisfy the requirements because they are not vacuum-compatible, their actuators engage in uncompensated motions that generate significant vibrations, and their operational lifetimes are too short. Going beyond the initial outer-space application, the present vacuum-compatible, fast-acting, long-life shutter units could also be used in terrestrial settings in which there are requirements for their special characteristics.

In designing these shutter units, unbalanced, electromagnetically driven mechanisms were replaced with balanced mechanisms that include commercial piezoelectric bending actuators. In each shutter unit, the piezoelectric bending actuators are configured symmetrically as opposing cantilever beams within a housing that contains integral mounts for lenses that focus a laser beam to a waist at the shutter location. In operation, the laser beam is blocked by titanium blades bonded near the free ends of the piezoelectric benders. The benders are driven by shaped electrical pulses with a maximum voltage differential of less than 60 V. Preliminary measurements indicate that rise and fall times are less than 1 ms.

The **Prototype Shutter Unit** contains titanium blades on the tips of opposing cantilever-beam piezoelectric bending actuators inside a housing. Lenses to focus a laser beam to a waist are mounted on the outside of the housing. The housing shown permits fine adjustment of the laser shutter in six degrees of freedom within the laser optical bench of the flight experiment.

This work was done by David Brinza, Donald Moore, Eric Hochberg, Tom Radey, and Albert Chen of Caltech for **NASA's Jet Propulsion Laboratory**. *Further information is contained in a TSP (see page 1).*

The software used in this innovation is available for commercial licensing. Please contact Don Hart of the California Institute of Technology at (818) 393-3425. Refer to NPO-40151.

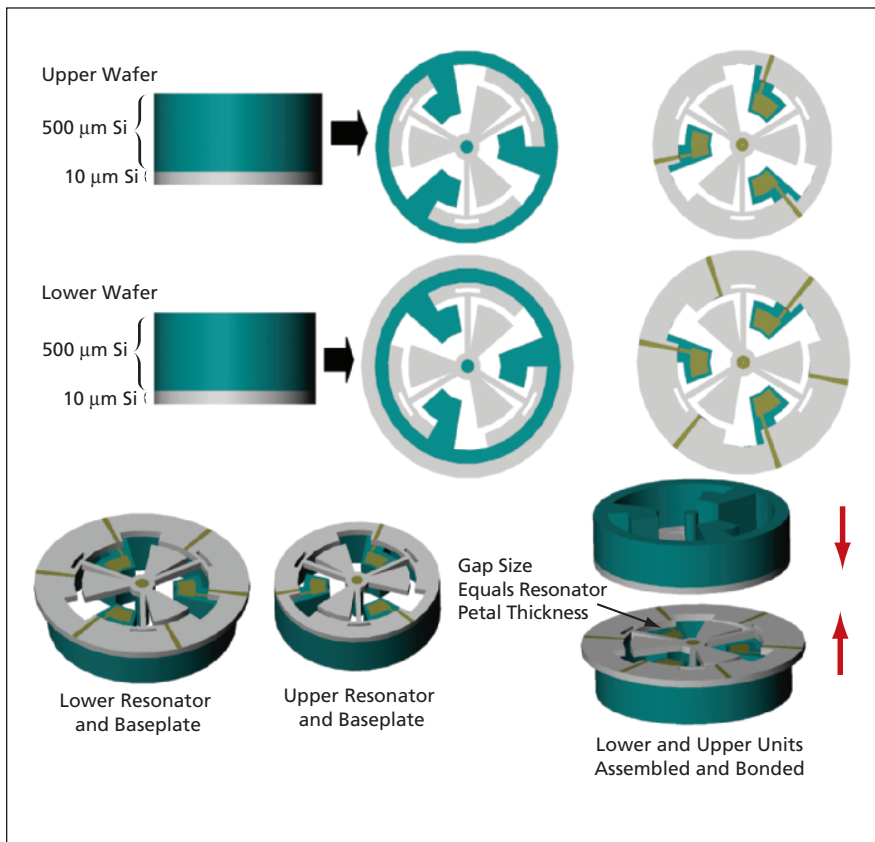# Split-Resonator, Integrated-Post Vibratory Microgyroscope

This design is better suited to mass production.

NASA's Jet Propulsion Laboratory, Pasadena, California

An improved design for a capacitive-sensing, rocking-mode vibratory microgyroscope is more amenable to mass production, relative to a prior design. Both the improved design and the prior design call for a central post that is part of a resonator that partly resembles a cloverleaf or a flower. The prior design is such that the post has to be fabricated as a separate piece, then bonded to the rest of the resonator in the correct position and orientation. The improved design provides for fabrication of the post as an integral part of the resonator and, in so doing, makes it possible to produce a waferful of microgyroscopes, without need to fabricate, position, and attach posts.

The improved design offers an additional advantage over the prior design with respect to the fact that the prior design calls for the post to be fabricated in upper and lower halves. The lower half post is fabricated as part of a baseplate in a lower wafer that is subsequently bonded to an upper wafer. Once the wafers are bonded, it is nec-

A **Split-Resonator, Integrated-Post Vibratory Microgyroscope** is made in upper and lower parts that are micromachined from two wafers, then bonded together.

ing processing time.

In the improved design (see figure), a resonator is split into an upper and a lower half, which are micromachined out of an upper and a lower wafer, respectively. A baseplate (which supports the resonator and is the relatively stationary object with respect to which the resonator vibrates) is likewise split into upper and lower halves. The upper and lower half resonators are offset from each other such that when the micromachined wafers are assembled and bonded together, the petals of the upper half resonator hang over electrodes on the lower half baseplate, while the petals of the lower half resonator hang over electrodes on the upper half baseplate. The capacitive gaps between the resonator petals and the baseplate are formed by opposing thicknesses of the half resonators.

essary to disconnect the lower half post from the baseplate. For mass production, it would be desirable to effect this disconnection by etching away the post support on the baseplate, but it is difficult to perform such an etch without damaging the microgyroscope, which, except for this etch, is complete at this stage. Therefore, instead of etching, it has proved necessary to perform ablation of individual supports, which entails processing time proportional to the number of microgyroscopes on a wafer. The improved design eliminates the need for ablation of individual supports, thereby correspondingly reducing processing time.

Blended Buffet-Load-Alleviation System for Fighter Airplane
Reductions in buffet loads translate to longer fatigue lives.

Langley Research Center, Hampton, Virginia

The capability of modern fighter airplanes to sustain flight at high angles of attack and/or moderate angles of sideslip often results in immersion of part of such an airplane in unsteady, separated, vortical flow emanating from its forebody or wings. The flows from these surfaces become turbulent and separated during flight under these conditions. These flows contain significant levels of energy over a frequency band coincident with that of low-order structural vibration modes of wings, fins, and control surfaces. The unsteady pressures applied to these lifting surfaces as a result of the turbulent flows are commonly denoted buffet loads, and the resulting vibrations of the affected structures are known as buffeting. Prolonged exposure to buffet loads has resulted in fatigue of structures on several airplanes. Damage to airplanes caused by buffeting has led to redesigns of airplane structures and increased support costs for the United States Air Force and Navy as well as the armed forces of other countries. Time spent inspecting, repairing, and replacing structures adversely affects availability of aircraft for missions.

A blend of rudder-control and piezoelectric-actuator engineering concepts was selected as a basis for the design of a vertical-tail buffet-load-alleviation system for the F/A-18 airplane. In this system, the rudder actuator is used to control the response of the first tail vibrational mode (bending at a frequency near 15 Hz), while directional patch piezoelectric actuators are used to control the second tail vibrational mode (tip torsion at a frequency near

45 Hz). This blend of two types of actuator utilizes the most effective features of each.

An analytical model of the aeroservoelastic behavior of the airplane equipped with this system was validated by good agreement with measured results from a full-scale ground test, flight-test measurement of buffet response, and an in-flight commanded rudder frequency sweep. The overall performance of the system was found to be characterized by reductions, ranging from 70 to 30 percent, in vertical-tail buffeting under buffet loads ranging from moderate to severe. These reductions were accomplished with a maximum commanded rudder angle of ±2° at 15 Hz and about 10 lb (≈4.5 kg) of piezoelectric actuators attached to the vertical tail skin and operating at a peak power level of 2 kW. By meeting the design objective, this system would extend the vertical-tail fatigue life beyond two aircraft lifetimes. This system is also adaptable to other aircraft surfaces and other aircraft.

Gifford-McMahon/Joule-Thomson Refrigerator Cools to 2.5 K

This system is relatively simple.

NASA's Jet Propulsion Laboratory, Pasadena, California

A compact refrigerator designed specifically for cooling a microwave maser low-noise amplifier is capable of removing heat at a continuous rate of 180 mW at a temperature of 2.5 K. This refrigerator is a combination of (1) a commercial Gifford-McMahon (GM) refrigerator nominally rated for cooling to 4 K and (2) a Joule-Thomson (J-T) circuit. The GM refrigerator pre-cools the J-T circuit, which provides the final stage of cooling. The refrigerator is compact and capable of operating in any orientation. Moreover, in comparison with a typical refrigerator heretofore used to cool a maser to 4.5 K, this refrigerator is simpler and can be built at less than half the cost.

The figure is a flow diagram of the refrigerator. The GM refrigerator comprises two stages. The first GM stage nominally provides 50 W of cooling power at a temperature of 50 K. The second GM stage nominally provides 1.5 W at 4.2 K. The working fluid of the J-T circuit is helium, which is supplied at ambient temperature at a pressure of 110 kPa. The J-T helium is circulated by means of a commercial scroll vacuum

pump that does not use any oil and hence does not contaminate the helium.

In the J-T circuit, the helium flowing toward a cold plate (the final, coldest stage) passes though a first-stage counterflow heat exchanger, where it is cooled by the helium in the return flow that has passed from the cold plate through a second-stage counterflow heat exchanger. The helium then passes through the first GM stage, where it is cooled to a temperature between 35 and 40 K. After the first GM stage, the helium flows through the second-stage counterflow heat exchanger, wherein it is cooled by helium returning from the cold plate. The helium then passes through the GM second stage, where it is cooled to between 3.5 and 4.2 K.
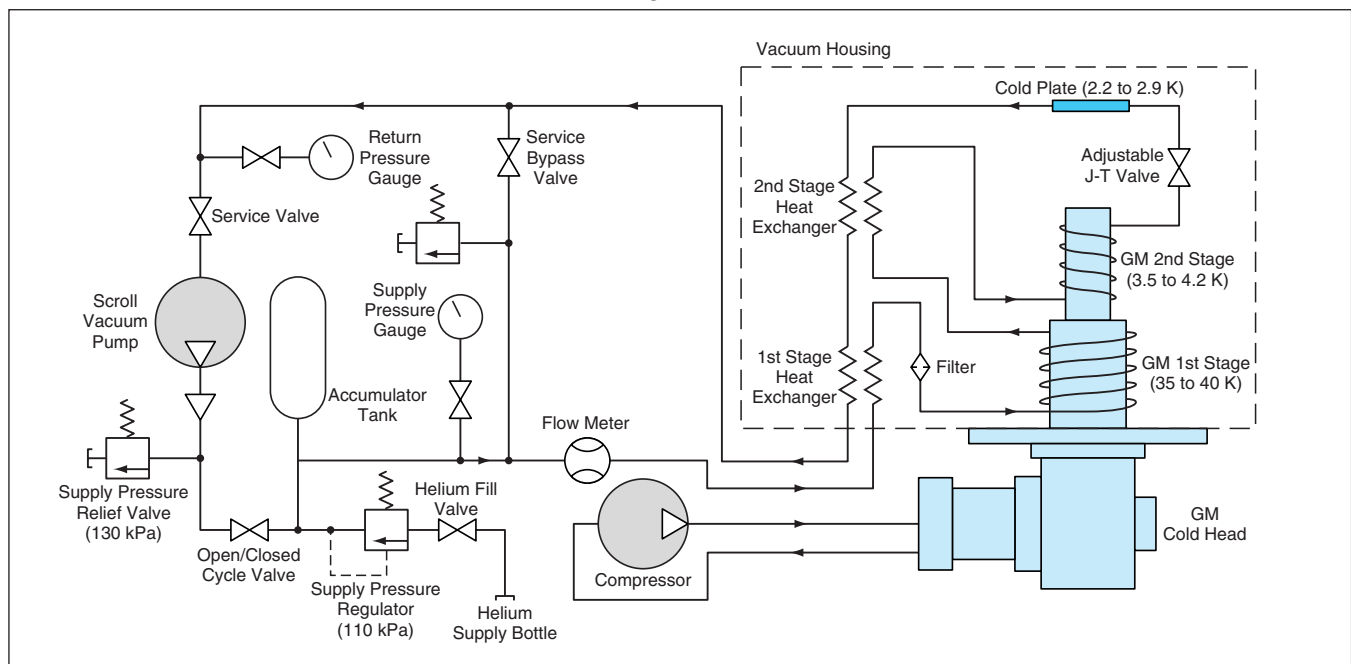
The flow is then throttled by means of an externally adjustable expansion valve (a J-T valve) to the final-stage (cold-plate) operating temperature and pressure. The temperature at the final stage is the saturation temperature of helium at the pressure in that stage. From the final stage, the helium returns through the heat exchangers as mentioned be-

fore, and is then compressed back to the supply pressure and recycled.

The cooling to ≤4.2 K in the GM second stage makes it possible to liquefy the helium immediately prior to the J-T expansion. This enables the refrigerator to operate without the third-stage heat exchanger that would otherwise be needed in the J-T circuit. Elimination of the third-stage heat exchanger reduces both the cool-down time and the complexity of the system.

During cool-down, helium is supplied from an external helium bottle through a regulator that maintains its pressure at 110 kPa. Once the cooler has reached thermal equilibrium, no more helium is supplied from the external bottle. Thereafter, an external buffer tank accommodates small changes in the helium pressure with changes in the cooling load, and an external relief valve prevents the pressure from rising above 130 kPa.

This **Refrigeration System** is a combination of a commercial Gifford-McMahon refrigerator and a simplified Joule-Thomson circuit.

✿ High-Temperature, High-Load-Capacity Radial Magnetic Bearing

Speed and temperature limits of rolling-element bearings can be exceeded.

John H. Glenn Research Center, Cleveland, Ohio

A radial heteropolar magnetic bearing capable of operating at a temperature as high as 1,000 °F (≈540 °C) has been developed. This is a prototype of bearings for use in gas turbine engines operating at temperatures and speeds much higher than can be withstood by lubricated rolling-element bearings.

It is possible to increase the maximum allowable operating temperatures and speeds of rolling-element bearings by use of cooling-air systems, sophisticated lubrication systems, and rotor-vibration-damping systems that are subsystems of the lubrication systems, but such systems and subsystems are troublesome. In contrast, a properly designed radial magnetic bearing can suspend a rotor without contact, and, hence, without need for lubrication or for cooling. Moreover, a magnetic bearing eliminates the need for a separate damping system, inasmuch as a damping function is typically an integral part of the design of the control system of a magnetic bearing.

The present high-temperature radial heteropolar magnetic bearing has a unique combination of four features that contribute to its suitability for the intended application:

1. The wires in its electromagnet coils are covered with an insulating material that does not undergo dielectric breakdown at high temperature and is pliable enough to enable the winding of the wires to small radii.
2. The processes used in winding and potting of the coils yields a packing factor close to 0.7 — a relatively high value that helps in maximizing the magnetic fields generated by the coils for a given supplied current. These processes also make the coils structurally robust.
3. The electromagnets are of a modular C-core design that enables replacement of components and semiautomated winding of coils.
4. The stator is mounted in such a manner as to provide stable support under radial and axial thermal expansion and under a load as large as 1,000 lb (≈4.4 kN).

In a test, the bearing was shown to suspend a rotor stably at a speed of 25,000 rpm at a temperature of 1,000 °F (≈540 °C). The static load capacity and power demand were measured as functions of supplied current, air gap, rotor speed, and temperature. Fault tolerance was demonstrated at 15,000 rpm and 1,000 °F (≈540 °C) by intentionally disabling power and maintaining a stably levitated rotor. At the time of reporting the information for this article, the bearing had withstood more than 30 hours of operation that included 18 thermal cycles up to 1,000 °F (≈540 °C). The bearing had also been operated for hundreds of hours at lower temperatures.

Fabrication of Spherical Reflectors in Outer Space

Process takes advantage of vacuum.

NASA's Jet Propulsion Laboratory, Pasadena, California

A process is proposed for fabrication of lightweight spherical reflectors in outer space for telescopes, radio antennas, and light collectors that would be operated there. The process would obviate the relatively massive substrates and frames needed to support such reflectors in normal Earth gravitation. According to the proposal, fabrication of a reflector would begin with blowing of a bubble to the specified reflector radius. Taking advantage of the outer-space vacuum as a suitable environment for evaporative deposition of metal, a metal-evaporation source would be turned on and moved around the bubble to deposit a reflective metal film over the specified reflector area to a thickness of several microns. Then the source would be moved and aimed to deposit more metal around the edge of the reflector area, increasing the thickness there to ≈100 μm to form a frame. Then the bubble would be deflated and peeled off the metal, leaving a thin-film spherical mirror having an integral frame. The mirror would then be mounted for use.

The feasibility of this technology has been proved by fabricating a prototype at JPL. As shown in the figure, a 2-in. (≈5-cm) diameter hemispherical prototype reflector was made from a polymer bubble coated with silver, forming a very smooth surface.

A **Prototype Reflector** was successfully produced, showing that the proposed fabrication is practicable.

*This work was done by Yu Wang, Jennifer Dooley, and Mark Dragovan of Caltech and Wally Serivens of the University of South Carolina for **NASA's Jet Propulsion Laboratory**. Further information is contained in a TSP (see page 1). NPO-30649*

Automated Rapid Prototyping of 3D Ceramic Parts

Unlike in prior rapid-prototyping processes, there is no manual stacking of sheets.

Marshall Space Flight Center, Alabama

An automated system of manufacturing equipment produces three-dimensional (3D) ceramic parts specified by computational models of the parts. The system implements an advanced, automated version of a generic rapid-prototyping process in which the fabrication of an object having a possibly complex 3D shape includes stacking of thin sheets, the outlines of which closely approximate the horizontal cross sections of the object at their respective heights. In this process, the thin sheets are made of a ceramic precursor material, and the stack is subsequently heated to transform it into a unitary ceramic object.

In addition to the computer used to generate the computational model of the part to be fabricated, the equipment used in this process includes:

• A commercially available laminated-object-manufacturing machine that was originally designed for building woodlike 3D objects from paper and was modified to accept sheets of ceramic precursor material, and

• A machine designed specifically to feed single sheets of ceramic precursor material to the laminated-object-manufacturing machine.

Like other rapid-prototyping processes that utilize stacking of thin sheets, this process begins with generation of the computational model of the part to be fabricated, followed by computational sectioning of the part into layers of predetermined thickness that collectively define the shape of the part. Information about each layer is transmitted to rapid-prototyping equipment, where the part is built layer by layer.

What distinguishes this process from other rapid-prototyping processes that utilize stacking of thin sheets are the details of the machines and the actions that they perform. In this process, flexible sheets of ceramic precursor material (called "green" ceramic sheets) suitable for lamination are produced by tape casting. The binder used in the tape casting is specially formulated to enable lamination of layers with little or no applied heat or pressure. The tape is cut into individual sheets, which are stacked in the

sheet-feeding machine until used. The sheet-feeding machine can hold enough sheets for about 8 hours of continuous operation.

A vacuum chuck in the sheet-feeding machine picks up a single green ceramic sheet. The sheet is then coated with a lamination-aiding material. The coated sheet is wrapped around a roller, on which it is transported into the laminated-object-manufacturing machine. There, the roller is actuated in such a manner as to laminate the coated sheet onto the stack of previously laminated and cut sheets.

Once the sheet has been thus incorporated as the top layer of the stack, control of the operation is passed back to the laminated-object-manufacturing machine. A carbon dioxide laser that is part of the laminated-object-manufacturing machine cuts the desired cross-sectional outline out of the top layer. (To make this possible, the laser operating parameters are adjusted, in accordance with the composition and thickness of the layers, so that only the top layer is cut.) The motion of the laser and thus the cutting path are determined by the computational specification of the cross-section represented by the just-added top layer.

The excess layer material lying outside the cross section is temporarily left in place to provide support as the 3D object is built. In addition to cutting the outline of the cross section, the laser cuts the excess layer material into tiles to facilitate removal of supporting material from around the 3D object after completion of the stack. After the cutting is finished, control is passed back to the sheet-feeding machine, which then laminates the next sheet onto the stack. The laminating and cutting steps are repeated until the stack is complete. The supporting material is then removed. Finally, the green ceramic stack is heat-treated in a furnace to remove the binder and sinter the ceramic to high density. This process has been used to make objects from diverse engineered ceramics, including alumina, zirconia, silicon carbide, aluminum nitride, silicon nitride, aluminum silicates, hydroxyapatite, and various titanates.

Tissue Engineering Using Transfected Growth-Factor Genes

Cells, matrices, and bioreactors are tailored to promote functional tissue engineering of cartilage.

Lyndon B. Johnson Space Center, Houston, Texas

A method of growing bioengineered tissues includes, as a major component, the use of mammalian cells that have been transfected with genes for secretion of regulator and growth-factor substances. In a typical application, one either seeds the cells onto an artificial matrix made of a synthetic or natural biocompatible material, or else one cultures the cells until they secrete a desired amount of an extracellular matrix. If such a bioengineered tissue construct is to be used for surgical replacement of injured tissue, then the cells should preferably be the patient's own cells or, if not, at least cells matched to the patient's cells according to a human-leucocyte-antigen (HLA) test. The bioengineered tissue construct is typically implanted in the patient's injured natural tissue, wherein the growth-factor genes enhance metabolic functions that promote the *in vitro* development of functional tissue constructs and their integration with native tissues. If the matrix is biodegradable, then one of the results of metabolism could be absorption of the matrix and replacement of the matrix with tissue formed at least partly by the transfected cells.

The method was developed for articular chondrocytes but can (at least in principle) be extended to a variety of cell types and biocompatible matrix materials, including ones that have been exploited in prior tissue-engineering methods. Examples of cell types include chondrocytes, hepatocytes, islet cells, nerve cells, muscle cells, other organ cells, bone- and cartilage-forming cells, epithelial and endothelial cells, connective-tissue stem cells, mesodermal stem cells, and cells of the liver and the pancreas. Cells can be obtained from cell-line cultures, biopsies, and tissue banks. Genes, molecules, or nucleic acids that secrete factors that influence the growth of cells, the production of extracellular matrix material, and other cell functions can be inserted in cells by any of a variety of standard transfection techniques.

The method was developed for polyglycolic acid scaffolds, but can (at least in principle) be extended to other biodegradable matrix materials, which include collagen, fibrin, and poly(lactic acid) [PLA], poly(glycolic acid) [PGA], and PLA/PGA copolymers. Non-biodegradable matrix materials include polystyrene, polyesters, polypropylene, and numerous other polymers. Preferably, the matrix for a given therapeutic application should be fabricated so as to have a microstructure similar to that of the extracellular matrix to be replaced. Mechanical loads imposed on the matrix by the surrounding tissue influence the cells on and in the matrix in such a manner as to promote the regeneration of an extracellular matrix that has the proper microstructure. The cross-link density of the matrix can be tailored in fabrication in order to tailor the mechanical properties of the matrix and, in the case of a biodegradable matrix, to tailor the rate of its biodegradation. The shape and size of the matrix and the implant made from it should, of course, be chosen to suit the implant site and tissue type. The matrix material can be coated with materials that promote specific adhesion and metabolic behavior of both transfected cells and native cells.

Another important consideration in the design of a matrix is porosity. Pores must be large enough that cells can reside within them and that nutrients can migrate to the cells and waste products can diffuse away from the cells. Typical pore sizes range from 50 to 300 µm; the size or range of sizes can be chosen to obtain the cell behavior and matrix properties desired for a given application. Moreover, the range of pore sizes for a given application can be chosen to promote a specific timetable and amount of vascular ingrowth from the surrounding tissue as well as migration of native cells.

This work was done by Henning Madry, Robert S. Langer, Lisa E. Freed, Stephen Trippel, and Gordana Vunjak-Novakovic of Massachusetts Institute of Technology for **Johnson Space Center**.

In accordance with Public Law 96-517, the contractor has elected to retain title to this invention. Inquiries concerning rights for its commercial use should be addressed to:

Technology Licensing Office
Massachusetts Institute of Technology
Five Cambridge Center, Kendall Square
Room NE25-230
Cambridge, MA 02142-1493
Phone: (617) 253-6966
Fax: (617) 258-6790
E-mail: tlo@mit.edu
Refer to MSC-23352, volume and number of this NASA Tech Briefs *issue, and the page number.*

Automation of Vapor-Diffusion Growth of Protein Crystals

High-throughput experiments are accelerated through automation of routine operations.

Marshall Space Flight Center, Alabama

Some improvements have been made in a system of laboratory equipment developed previously for studying the crystallization of proteins from solution by use of dynamically controlled flows of dry gas. The improvements involve mainly (1) automation of dispensing of liquids for starting experiments, (2) automatic control of drying of protein solutions during the experiments, and (3) provision for automated acquisition of video images for monitoring experiments in progress and for post-experiment analysis.

The automation of dispensing of liquids was effected by adding an automated liquid-handling robot that can aspirate source solutions and dispense them in either a hanging-drop or a sitting-drop con-

figuration, whichever is specified, in each of 48 experiment chambers. A video camera of approximately the size and shape of a lipstick dispenser was added to a mobile stage that is part of the robot, in order to enable automated acquisition of images in each experiment chamber. The experiment chambers were redesigned to enable the use of sitting drops, enable backlighting of each specimen, and facilitate automation.

The evaporation of water from the protein solution in each chamber can be controlled independently of the evaporation in the other chambers. Hence, a total of 48 unique evaporation-rate-versus-time profiles can be tested simultaneously. Interface software was written for use in controlling all aspects of operation of the system. The software also enables the user to specify the evaporation profile for each chamber and provides for automatic acquisition of the images from each experiment chamber and the storage of the images for later analysis.

Atom Skimmers and Atom Lasers Utilizing Them

Atom skimmers act as conduits and low-pass velocity filters.

John H. Glenn Research Center, Cleveland, Ohio

Atom skimmers are devices that act as low-pass velocity filters for atoms in thermal atomic beams. An atom skimmer operating in conjunction with a suitable thermal atomic-beam source (e.g., an oven in which cesium is heated) can serve as a source of slow atoms for a magneto-optical trap or other apparatus in an atomic-physics experiment. Phenomena that are studied in such apparatuses include Bose-Einstein condensation of atomic gases, spectra of trapped atoms, and collisions of slowly moving atoms.

An atom skimmer (see figure) includes a curved, low-thermal-conduction tube that leads from the outlet of a thermal atomic-beam source to the inlet of a magneto-optical trap or other device in which the selected low-velocity atoms are to be used. Permanent rare-earth magnets are placed around the tube in a yoke of high-magnetic-permeability material to establish a quadrupole or octupole magnetic field leading from the source to the trap. The atoms are attracted to the locus of minimum magnetic-field intensity in the middle of the tube, and the gradient of the magnetic field provides centripetal force that guides the atoms around the curve along the axis of the tube. The threshold velocity for guiding is dictated by the gradient of the magnetic field and the radius of curvature of the tube. Atoms moving at lesser velocities are successfully guided; faster atoms strike the tube wall and are lost from the beam.

In the example of the figure, the magnets are made of NdFeB, a material that provides the largest fields. The inner diameter of the tube is 1.1 cm and the total arc length is 25 cm. Although a larger diameter could result in a greater flux of slow atoms, a smaller diameter provides a higher degree of thermal and pressure isolation between the source chamber and the trap chamber, which must be maintained cold and at ultrahigh vacuum. The entrance solid angle for the thermal beam is improved by extending the octupole magnetic field to inside the source chamber. The magnets in the source chamber are made of SmCo because the Curie temperature of this material is high enough to make it possible to retain magnetism while vacuum-baking the magnets along with the chamber. The high-magnetic-permeability yoke material in this design is a 400-series stainless steel. The yokes shunt the field lines, reducing stray fields that might perturb the tr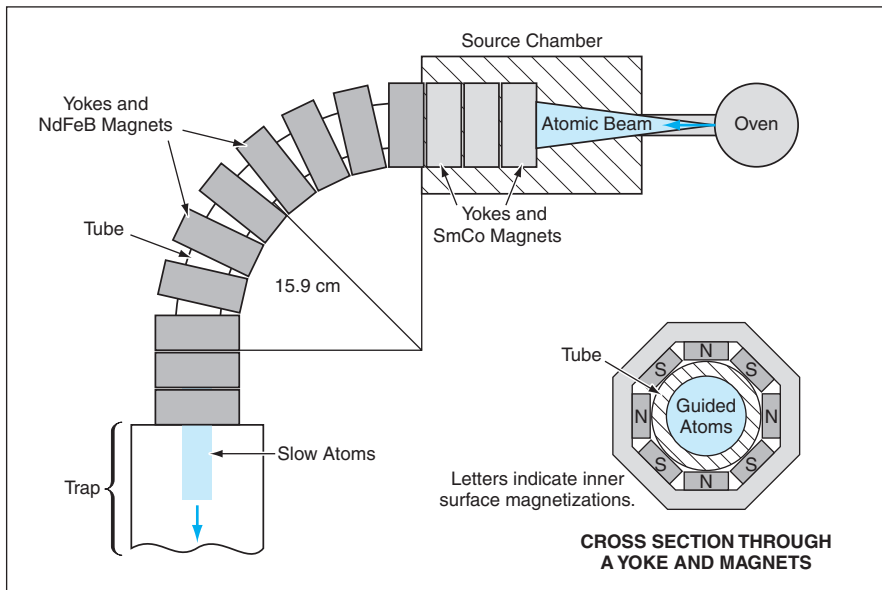ap. They also flatten the magnetic-field profile, thereby widening the entrance for slow atoms. The yokes also increase the magnetic-field strength by about 50 percent in the guiding region inside the tube and serve as a frame for holding the magnets in the appropriate positions.

According to a proposal, atom skimmers would be utilized as coupling devices in atom-laser systems. An atom laser is a conceptual device, based partly on the concept of a Bose-Einstein condensate, which is a collection of many atoms that have exactly the same energy or, equivalently, are in the same quantum state. Atom lasers would be analogous to optical lasers in some respects. Like beams of laser light, beams of atoms drawn from Bose-Einstein condensates exhibit coherence and interference. Potential systems based on atom lasers could include atomic interferometers as rotation sensors and gravity gradiometers, sources of atoms for precisely controlled deposition, and improved atomic clocks. The role of atom skimmers in atom-laser systems could be analogous to that of optical fibers in optical systems.

The atom-skimmer concept is amenable to miniaturization. The magnetic fields needed for guiding could be generated by magnetic thin films deposited on substrates or by electromagnets in the form of microfabricated wires carrying electric currents. Hence, such systems as atomic interferometers fed by atom lasers and using magnetic guiding of atom-laser outputs could be fabricated with dimensions and by use of techniques similar to those of integrated circuits.

An **Atom Skimmer** consists basically of a curved tube surrounded by magnets that generate a multipole magnetic field. Low-velocity atoms are guided along the tube from the source to the trap.
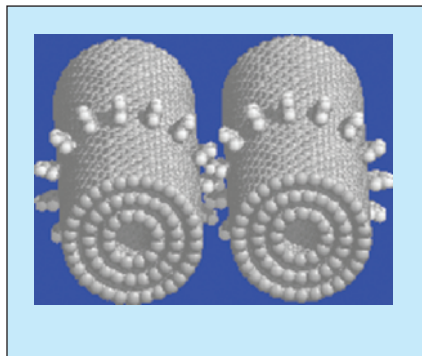
Gears Based on Carbon Nanotubes

Nanometer size gears could be used in molecular-scale machines.

Ames Research Center, Moffett Field, California

Gears based on carbon nanotubes (see figure) have been proposed as components of an emerging generation of molecular-scale machines and sensors. In comparison with previously proposed nanogears based on diamondoid and fullerene molecules, the nanotube-based gears would have simpler structures and are more likely to be realizable by practical fabrication processes. The impetus for the practical development of carbon-nanotube-based gears arises, in part, from rapid recent progress in the fabrication of carbon nanotubes with prescribed diameters, lengths, chiralities, and numbers of concentric shells.

The shafts of the proposed gears would be made from multiwalled carbon nanotubes. The gear teeth would be rigid molecules (typically, benzyne molecules), bonded to the nanotube shafts at atomically precise positions. For fabrication, it may be possible to position the molecular teeth by use of scanning tunneling microscopy (STM) or other related techniques. The capability to position individual organic molecules at room temperature by use of an STM tip has already been demonstrated. Routes to the chemical synthesis of carbon-nanotube-

Two Molecular-Scale Gears are shown meshing in this computer-simulation image. The gears would include multiwalled carbon-nanotube shafts, to which gear teeth in the form of benzyne molecules would be bonded.

based gears are also under investigation.

Chemical and physical aspects of the synthesis of molecular scale gears based on carbon nanotubes and related molecules, and dynamical properties of nanotube-based gears, have been investigated by computational simulations using established methods of quantum chemistry and molecular dynamics. Several particularly interesting and useful conclusions have been drawn from the dynamical simulations performed thus

far: The forces acting on the gears would be more sensitive to local molecular motions than to gross mechanical motions of the overall gears. Although no breakage of teeth or of chemical bonds is expected at temperatures up to at least 3,000 K, the gears would not work well at temperatures above a critical range from about 600 to about 1,000 K. Gear temperature could probably be controlled by use of coolant gases. For a given application, the gears would work well at temperatures below the critical range, provided that the rotational energy was less than the energy required to tilt the teeth through an angle of 20°. The predominant mechanism of gear failure would be slippage caused by tilting of teeth. Gears would resume functioning if the slipping gears were decelerated sufficiently.

This work was done by Richard Jaffe of **Ames Research Center***; Jie Han and Al Globus of MRJ, Inc.; and Glenn Deardorff of Sterling Software. Further information is contained in a TSP (see page 1).*

Inquiries concerning rights for the commercial use of this invention should be addressed to the Patent Counsel, Ames Research Center, (650) 604-5104. Refer to ARC-15116-1.

Books & Reports

Patched Off-Axis Bending/Twisting Actuators for Thin Mirrors

Two documents present updates on thin-shell, adjustable, curved mirrors now being developed for use in space-borne imaging systems. These mirrors at an earlier stage of development were reported in "Nanolaminate Mirrors With Integral Figure-Control Actuators" (NPO-30221), *NASA Tech Briefs*, Vol. 26, No. 5 (May 2002), page 80. To recapitulate: These mirrors comprise metallic film reflectors on nanolaminate substrates that contain "in-plane" actuators for controlling surface figures with micron-level precision. The actuators are integral parts of the mirror structures, typically fabricated as patches that are bonded onto the rear (nonreflective) surfaces of the mirror shells. The current documents discuss mathematical modeling of mirror deflections caused by actuators arranged in unit cells distributed across the rear mirror surfaces. One of the documents emphasizes an actuator configuration in which a mirror surface is divided into hexagonal unit cells. Each unit cell contains four rectangular actuator patches in an off-axis cruciform pattern to induce a combination of bending and twisting. For deflections to reduce certain optical aberrations, it is found that, relative to other configurations, this configuration involves a smaller areal density of actuators.

This work was done by Gregory Hickey, Shyh-Shiuh Lih, and Horn-Sen Tzou of Caltech for **NASA's Jet Propulsion Laboratory**. *Further information is contained in a TSP (see page 1).*
NPO-30748

Improving Control in a Joule-Thomson Refrigerator

A report discusses a modified design of a Joule-Thomson (JT) refrigerator under development to be incorporated into scientific instrumentation aboard a spacecraft. In most other JT refrigerators (including common household refrigerators), the temperature of the evaporator (the cold stage) is kept within a desired narrow range by turning a compressor on and off as needed. This mode of control is inadequate for the present refrigerator because a JT-refrigerator compressor performs poorly when the flow from its evaporator varies substantially, and this refrigerator is required to maintain adequate cooling power. The proposed design modifications include changes in the arrangement of heat exchangers, addition of a clamp that would afford a controlled heat leak from a warmer to a cooler stage to smooth out temperature fluctuations in the cooler stage, and incorporation of a proportional + integral + derivative (PID) control system that would regulate the heat leak to maintain the temperature of the evaporator within a desired narrow range while keeping the amount of liquid in the evaporator within a very narrow range in order to optimize the performance of the compressor. Novelty lies in combining the temperature- and cooling-power-regulating controls into a single control system.

This work was done by James Borders, David Pearson, and Mauro Prina of Caltech for **NASA's Jet Propulsion Laboratory**. *Further information is contained in a TSP (see page 1).*
NPO-40225

National Aeronautics and
Space Administration